Endocytosis sculpts distinct cAMP signal transduction by endogenously coexpressed GPCRs

Emily E Blythe[1,2]*, Rita R Fagan[1], and Mark von Zastrow[1,3,4]*

[1]Department of Psychiatry and Behavioral Sciences, University of California, San Francisco, San Francisco, CA, USA.
[2]Department of Genetics, Cell Biology and Development, University of Minnesota, Minneapolis, MN, USA
[3]Department of Cellular and Molecular Pharmacology, University of California, San Francisco, San Francisco, CA, USA.
[4]Quantitative Biology Institute, University of California, San Francisco, San Francisco, CA, USA
*Correspondence: eblythe@umn.edu, mark.vonzastrow@ucsf.edu

Abstract

Many G protein-coupled receptors (GPCRs) trigger a second phase of G protein-dependent signaling from internal membranes after agonist-induced endocytosis. However, individual GPCRs differ significantly in their ability to internalize, and it remains unclear if this confers selectivity on cellular signaling through natively coexpressed GPCRs. We addressed this question by examining the activation of the cyclic AMP (cAMP) / cAMP-dependent protein kinase (PKA) pathway by three ligands that stimulate three distinct, endogenously coexpressed GPCRs in HEK293 cells: isoproterenol (Iso) which primarily activates the β2-adrenergic receptor (β2AR), vasoactive intestinal peptide (VIP) which primarily activates the VIP receptor 1 (VIPR1/VPAC1), and 5'-N-ethylcarboxamidoadenosine (NECA) which primarily activates the adenosine 2B receptor ($A_{2B}R$). Using location-targeted biosensors and a transcriptional reporter, we demonstrate that each ligand triggers a unique cellular signaling profile and that these responses are differentially sensitive to endocytic inhibition. VIP elicited a response that was endocytosis-dependent at every level in the pathway, from upstream global cAMP elevation to downstream activation of nuclear PKA, while Iso elicited a response that was dependent on endocytosis selectively at downstream steps. In contrast, NECA robustly activated the entire cAMP signaling cascade independently of endocytosis, consistent with our observation that human $A_{2B}R$ does not robustly internalize after activation. We conclude that endocytosis indeed sculpts downstream cAMP signaling by GPCRs in a receptor-specific manner. Our results add to the evolving view of compartmentalized signaling in the cAMP / PKA pathway and suggest that differences in GPCR trafficking can encode receptor-specific signaling profiles through a shared signal transduction pathway.

Introduction

Cells sense their chemical environment through membrane-embedded receptors that communicate ligand binding to elicit appropriate downstream cellular responses. The largest family of such chemical detectors in animal cells are the G protein-coupled receptors (GPCRs), integral membrane proteins that relay information through the allosteric activation of four families of heterotrimeric G proteins (*1*). Mammalian cells characteristically coexpress a large repertoire of GPCRs (e.g. (*2*)), enabling them to distinguish a diversity of ligands that far exceeds the diversity of G protein subtypes available for signal transduction. Previous work in cell culture models and tissues has demonstrated that natively coexpressed GPCRs that couple to the same G proteins can generate unique patterns of signaling (*3–5*) and physiological responses (*6*). This observation suggests that cellular ligand discrimination cannot be based solely on the inherent biochemical specificity of GPCR-G protein coupling, raising a fundamental question of how additional selectivity is achieved using a shared signaling network.

One strategy for ligand discrimination is to segregate GPCRs into different regions of the plasma membrane with their relevant signaling partners, effectively leveraging the plasma membrane as a two-dimensional surface for the lateral organization of signaling pathways (*1*, *7*). A second strategy is to compartmentalize signaling in three dimensions between the plasma membrane and other membranes. For example, many GPCRs are now known to also activate G proteins from endomembranes after agonist-induced internalization (*8*). This paradigm of endomembrane GPCR signaling is particularly well-developed for receptors that couple to Gs to increase intracellular levels of cAMP and produce downstream effects through a complex effector network regulated by cAMP-mediated activation of cAMP-dependent protein kinase (PKA) (*9*). Lateral organization of PKA signaling complexes on the plasma membrane, particularly by A-kinase anchoring proteins (AKAPs), has been recognized for many years (*7*, *10*), and there is now considerable evidence linking specific downstream outcomes of GPCR-mediated cAMP signaling, including PKA-mediated transcriptional activation, to activity of receptors at endomembranes (*8*, *11–14*).

It is well known that individual GPCRs differ in their membrane trafficking properties, particularly in their tendencies to internalize after activation (*15–17*). Accordingly, we wondered if regulated endocytosis confers an additional dimension of selectivity on the downstream cellular signaling profiles initiated through distinct GPCRs that are natively coexpressed. Endocytosis has been demonstrated previously to impact the cellular signaling profile of individual GPCRs when studied in isolation, and often under conditions of heterologous overexpression (*8*). However, to our knowledge, whether endocytosis confers significant selectivity on cellular ligand detection mediated by endogenously coexpressed GPCRs remains to be tested. Do individual GPCRs that are natively coexpressed differentially leverage endocytic trafficking to encode ligand-specific signaling profiles?

Here, we explicitly investigate this question by focusing on cAMP signaling outcomes triggered by chemically diverse ligands that activate Gs-coupled GPCRs natively coexpressed in HEK293 cells. Specifically, we compare the effects of isoproterenol (Iso), which primarily signals through the β2-adrenergic receptor (β2AR); vasoactive intestinal peptide (VIP), which primarily signals through the vasoactive intestinal peptide receptor 1 (VIPR1/VPAC1); and 5'-N-ethylcarboxamidoadenosine (NECA), which primarily signals through the adenosine 2B receptor ($A_{2B}R$). Our results indicate that endocytosis strongly promotes downstream signaling elicited by both Iso and VIP, consistent with the previously established ability of both the β2AR and VIPR1 to robustly internalize after agonist-induced activation. However, the degree to which endocytosis sculpts each step in the cAMP/PKA pathway differs between receptors. VIPR1 relies on internalization to promote signaling at all steps in the pathway while β2AR endocytosis affects primarily downstream PKA signaling. In contrast, NECA-induced activation of $A_{2B}R$, which we show here internalizes poorly compared to β2AR and VIPR1, strongly promotes signaling through the cAMP / PKA pathway without detectable dependence on endocytosis at any step. Our results demonstrate that endocytosis indeed contributes to functional ligand discrimination through GPCRs and suggest a simple cellular scheme for how this element of selectivity is encoded.

Results

β2AR, VIPR1, and $A_{2B}R$ are natively coexpressed but differ in their agonist-induced trafficking

To explore the diversity of GPCR-mediated cAMP signaling and trafficking, we first sought to identify Gs-coupled receptors that are endogenously coexpressed in our HEK293 cell model (Figure 1A). Studies have reported HEK293 sensitivity to the non-selective β-adrenergic receptor (βAR) agonist Iso, the hormone VIP, and the adenosine analog 5'-N-ethylcarboxamidoadenosine (NECA) (*12*, *18*, *19*). We previously identified VIPR1 as the predominant GPCR mediating VIP-stimulated cAMP production our HEK293 system (*20*), and we employed pharmacological and genetic approaches to characterize the Iso- and NECA-sensitive GPCRs coexpressed in

these cells. Using subtype-selective βAR antagonists (CGP 20712 for β1AR and ICI 118551 for β2AR) (*21*, *22*), we found the β2AR to be the predominant GPCR mediating Iso-stimulated cAMP cascade activation in the cells used in the present study (Supplementary Figure 1). NECA sensitivity in HEK293 has been previously attributed to expression of $A_{2B}R$ (*19*), and indeed, CRISPR knockout of $A_{2B}R$ largely abolished the NECA-stimulated cAMP response in our HEK293 system (Supplementary Figure 2A-B). Furthermore, application of CGS-21680, a potent and selective agonist for the adenosine 2A receptor ($A_{2A}R$), the other Gs-coupled adenosine receptor subtype, did not substantially stimulate cAMP production (Supplementary Figure 2C). Together, these results suggest that $A_{2B}R$ is the predominant GPCR mediating NECA-triggered activation of the cAMP cascade in our system.

Next, we asked if these GPCRs differ in their tendency to rapidly internalize after agonist-induced activation. To do so, we used a flow cytometry-based internalization assay that uses a cell-impermeant HaloTag dye (JF_{635}i-HTL) (*23*) to measure the effect of agonist application on plasma membrane levels of N-terminally HaloTagged receptors. Using this method, and consistent with previous reports (*18*, *20*, *24*), we observed agonist-induced internalization of the human β2AR and VIPR1 (Figure 1B). We were unable to detect any internalization of the human $A_{2B}R$ over 30 minutes using the same halo-tag assay system (Figure 1B). Similar results were obtained by an analogous method using a FLAG-tagged human $A_{2B}R$ (Supplementary Figure 3). We note that agonist-induced internalization of a rat $A_{2B}R$ was previously demonstrated in HEK293 cells (*25*), but our results indicate that the human $A_{2B}R$ internalizes much less robustly than the VIPR1 or β2AR in our system.

Following internalization, β2AR and VIPR1 initiate a second wave of Gs-mediated signaling at the endosome (*20*, *26*). Since $A_{2B}R$ does not detectably internalize, we anticipated that it produces less signaling from endomembranes than β2AR or VIPR1. To test this, we assessed receptor recruitment of mini-Gs (mG_s), a minimal G protein that reports on the receptor active state conformation (*27*, *28*). Venus-tagged mG_s was co-expressed with N-terminally FLAG-tagged receptors which were labeled at the cell surface using a fluorescent anti-FLAG antibody. For all three GPCRs, we observed agonist-dependent recruitment of mini-G_s to the cell surface, indicative of agonist-induced activation at the plasma membrane (Figure 1C). We also observed internal puncta of FLAG-labeled β2AR and VIPR1, indicative of receptor-containing endosomes. These structures colocalized with mini-G_s, supporting the previous conclusion that β2AR and VIPR1 signal from endosomes as well as the plasma membrane (*20*, *26*). However, this was not the case for $A_{2B}R$. Here, we observed FLAG-labeled puncta both in the presence and absence of NECA, suggesting some constitutive (agonist-independent) internalization, but these puncta did not colocalize with mini-G_s. While we cannot rule out some contribution of endosomes to the overall cellular response to NECA mediated through the human $A_{2B}R$, these results strongly suggest that the human $A_{2B}R$ produces little or no endosomal signal compared to the human β2AR and VIPR1.

Endogenous β2AR, VIPR1, and $A_{2B}R$ exhibit distinct signaling dynamics

Because these three endogenously coexpressed GPCRs differ significantly both in regulated internalization and evidence for activation in endosomes, we were next curious how these differences might affect temporal patterns of signaling elicited by Iso, VIP, and NECA through the cAMP pathway. To characterize signaling over time in HEK293 cells, we employed genetically encoded fluorescent biosensors that respond to intracellular levels of cAMP (cADDis) or PKA activity (ExRai-AKAR2) (*29*). Importantly, these experiments were performed without overexpression of tagged receptors and measure signaling generated from endogenous receptor pools. While we probed these two responses over a range of agonist concentrations (Supplementary Figure 4A), we have chosen to focus our discussion on signaling patterns prompted by saturating concentrations of Iso, VIP, and NECA for simplicity (Supplementary Figure 4B, Supplementary Table 1).

We first probed changes in intracellular cAMP and observed distinct temporal profiles of cAMP elevation upon stimulation of the three receptors. Qualitatively, the initial Iso response decreased gradually across the entire time course; the VIP response rapidly peaked, exhibited a small and brief second increase, and plateaued (*20*); and the NECA response remained largely sustained (Figure 2A). While all three agonists triggered similar peak levels of cAMP (Figure 2A, Supplementary Figure 5A), their desensitization differed greatly, with decay constants that varied up to ~30-fold (Supplementary Table 2). To summarize these complex dynamics, we calculated a sustained activity metric (*30*), which compares the signal remaining at 30 minutes post agonist addition to the peak signal. Using this metric, consistent with our qualitative analysis, we found that NECA elicited the most sustained cAMP response, while VIP elicited the most transient response (Supplementary Figure 5B).

Next, we assessed the downstream PKA response. Regarding global cellular PKA activity, the three agonists triggered temporal patterns of PKA activity that closely mirror their cAMP responses (Figure 2B), and this observation is supported by comparable measures of peak and sustained signaling (Supplementary Figure 5A-B). PKA activity can also be compartmentalized in the cell (*7*, *10*). To specifically probe nuclear PKA activity, we expressed a version of the PKA biosensor with a nuclear localization signal (ExRai-AKAR2-NLS). Here, responses among agonists remained distinct from one another but displayed muted dynamics compared to their cytoplasmic responses (Figure 2C). All three agonists were significantly slower in reaching their peak nuclear PKA activities than their peak cAMP responses (Supplementary Figure 5C). Additionally, the nuclear PKA responses were significantly more sustained than their upstream global cAMP and PKA signals for all three agonists (Supplementary Figure 5B), partly due to the apparent suppression of a rapid initial peak in signal (Figure 2A vs 2C) and partly due to slower rates of signaling decay (Supplementary Table 2). This behavior, akin to a low pass filter, has been observed previously in a variety of cell types and is regulated by factors including PKA diffusion rates, nuclear protein kinase inhibitor, and the compartmentalized activities of phosphodiesterases and phosphatases (*31–34*). In sum, native HEK293 cells display unique temporal patterns of signaling at multiple steps in the cAMP / PKA pathway depending on the type of ligand stimulation.

Endocytosis has receptor-specific effects on prolonged signaling

Given the unique signaling dynamics elicited by the three ligands and the different trafficking behaviors of their cognate GPCRs, we wondered to what degree receptor trafficking, specifically receptor endocytosis, is responsible for dictating downstream signaling. To probe the relationship between trafficking and signaling, we inhibited endocytosis by overexpressing a dominant negative mutant of dynamin (DynK44E). Because DynK44E has previously been shown to block the agonist-induced internalization of β2AR and VIPR1 (*18*, *20*, *35*), we hypothesized that this perturbation would diminish signaling through these two receptors but not affect signaling through the minimally internalizing $A_{2B}R$. To test this, we analyzed the effects of DynK44E on global intracellular cAMP as well as compartmentalized PKA activity via the expression of the nuclear PKA biosensor and a version of the same biosensor localized to the cytoplasm by a nuclear export signal (ExRai-AKAR2-NES).

Across all sensors and all agonists, we observed a significant decrease in the magnitude of signaling upon 24-hour expression of mCherry-DynK44E compared to an mCherry control (Supplementary Figures 6-8). However, we did not observe a similar universal suppression of signaling when we subjected cells to acute endocytic inhibition with a 10-minute pretreatment of the dynamin inhibitor Dyngo4a (Supplementary Figure 9A)(*20*), suggesting that this decrease may be a pleiotropic effect of prolonged endocytic inhibition. When we normalized each time course to its maximum signal, the effects of prolonged endocytic inhibition via DynK44E closely mirrored those of acute endocytic inhibition via Dyngo4a (Supplementary Figure 9B-C). Dyngo4a treatment leads to cell toxicity upon prolonged treatment; thus, we moved forward with DynK44E but used this method of normalization to correct for its global effects on signaling.

Expression of DynK44E revealed key differences in how endocytic inhibition affected signaling by the three agonists. Starting at the beginning of the cascade, we found that endocytic inhibition did not qualitatively alter the time course of Iso- or NECA-stimulated cAMP production but did abolish VIP-stimulated cAMP production at later timepoints (Figure 3A). To more clearly visualize the effect of endocytosis, we calculated the difference between the control and DynK44E curves over time, which we interpret to be the fraction of cAMP signaling that is dependent on endocytosis. This differential cAMP fluctuates around zero for Iso and NECA stimulation but markedly increases over time for VIP stimulation (Figure 3B), consistent with substantial cAMP production downstream of internalized VIPR1. Indeed, when we integrated this cAMP signaling over time, we found that ~60% of VIP-mediated cAMP signaling is dependent on endocytosis, compared to ~10% through Iso or NECA (Figure 3C). These differences are also evident as a significant DynK44E-dependent reduction in sustained cAMP elicited by VIP but not by Iso or NECA (Figure 3D).

To determine how later steps in the cAMP cascade are sculpted by endocytosis, we next examined how DynK44E expression affected cytoplasmic PKA activity. Similar to cAMP, cytoplasmic PKA activity from NECA was only moderately suppressed by endocytic inhibition (Figure 4A), displaying a non-zero but small endocytic component of signaling that did not change over time (Figure 4B). Also consistent with upstream cAMP, VIP-stimulated cytoplasmic PKA activity displayed a strong endocytic component to signaling at later timepoints (Figure 4A-B). In contrast, Iso exhibited distinct responses to DynK44E at the level of cytoplasmic PKA activity compared to cAMP. Whereas DynK44E expression had no significant effect on cAMP signaling, it caused a loss of PKA signaling at later timepoints (Figure 4A), resulting in a rise in the endosomal component of PKA activity that was comparable to that of VIP 30 minutes after agonist addition (Figure 4B). Consequently, the endosomal component of integrated cytoplasmic PKA signaling remained the largest through VIP, followed by Iso, and then NECA (Figure 4C). While DynK44E expression led to a minor but statistically significant loss of NECA-stimulated sustained signaling (~15%), Iso- and VIP-stimulated sustained signaling were more drastically dampened (~40% and ~60%, respectively) (Figure 4D).

These trends in cytoplasmic PKA activity were also observed at the level of nuclear PKA activity. NECA signaling dynamics were largely unperturbed by DynK44E expression (Figure 5A-B). We observed virtually no endocytic component to integrated nuclear PKA activity (Figure 5C), and there was no significant difference in sustained signaling upon endocytic inhibition (Figure 5D). However, signaling from both Iso and VIP was again suppressed at later timepoints by endocytic inhibition (Figure 5A), revealing a prominent endocytic component to nuclear PKA activity (Figure 5B-C). Like cytoplasmic PKA signaling, Iso- and VIP-stimulated sustained nuclear PKA signaling were significantly suppressed by endocytic inhibition (Figure 5D).

Consistent with receptor trafficking, these data together suggest that Iso/β2AR- and VIP/VIPR1-mediated signal transduction is sculpted by endocytosis, whereas NECA/A_{2B}R-mediated signal transduction is largely unaffected by endocytosis. Specifically, β2AR and VIPR1 rely on receptor trafficking to support prolonged cAMP and/or PKA signaling while A_{2B}R can promote prolonged signaling in the absence of endocytosis.

NECA elicits a strong endocytosis-independent transcriptional response

Given these differences, we were curious how endocytosis further shapes GPCR-mediated responses downstream of PKA. One target of nuclear PKA is the cyclic AMP-responsive element-binding protein (CREB), a transcription factor that promotes transcriptional activation by binding to a cyclic AMP response element (CRE). To assess transcription downstream of CREB, we employed a transcriptional reporter assay composed of luciferase under the control of a CRE. As expected, we observed an increase in luminescence after a 5 hour

treatment with each agonist, indicating GPCR-mediated CREB activation (Figure 6A, Supplementary Figure 10A). Interestingly, NECA treatment produced the strongest induction of luciferase compared to Iso or VIP. Consistent with this observation, NECA treatment also induced higher levels of CREB phosphorylation (Supplementary Figure 10B) and more changes in the transcriptome, as measured by RNA sequencing-based differential gene expression analysis (Supplementary Figure 10C, Supplementary Table 3), compared to treatment with Iso or VIP.

Endocytic inhibition had receptor-specific effects on transcriptional activation. Both Iso- and VIP-stimulated induction of luciferase were strikingly blunted by DynK44E overexpression, displaying ~40% and ~60% reduction, respectively (Figure 6B-C). In contrast, NECA-stimulated induction of luciferase was largely insensitive to DynK44E (Figure 6D). The difference in luminescence between DynK44E and control was relatively small (up to ~15%) and only reached statistical significance for one concentration of NECA. Thus, similar to its effects on upstream cAMP and PKA signaling, endocytosis was critical to dictating transcriptional responses through Iso/β2AR and VIP/VIPR1 but not through NECA/A_{2B}R.

Discussion

Our results explicitly demonstrate that endocytosis sculpts distinct spatiotemporal signaling profiles by endogenously coexpressed GPCRs that couple to the same G protein pathway, thereby contributing to the selectivity of cellular ligand discrimination. By assessing separate steps of the canonical cAMP/PKA pathway, we show that chemically diverse ligands stimulating distinct endogenous GPCRs elicit unique signaling profiles through a shared downstream signal transduction pathway and that these profiles are differentially sculpted by receptor endocytosis. Accordingly, we demonstrate that receptor-specific trafficking differences indeed contribute to determining the downstream signaling profiles of cellular ligand discrimination through endogenously co-expressed GPCRs.

For Iso and VIP, the two ligands that produce transient cAMP elevations at the plasma membrane and drive cognate receptor internalization, endocytosis was found to strongly potentiate downstream signaling. The endosomal signals elicited by Iso and VIP were not identical, however, as they differed in how far upstream in the pathway they were detected, conferring additional diversity. Because VIPR1 is rapidly and robustly desensitized at the plasma membrane, a second wave of activity at the endosome is critical for continuing cAMP/PKA signaling at all levels. β2AR desensitization at the plasma membrane appears to be less rapid and complete, however, as endocytic blockade has minimal effects on global intracellular cAMP levels. Yet, we still observed a clear dependence of sustained PKA activity and transcriptional activation on endocytosis.

Previous studies of individual GPCRs and engineered adenylyl cyclases have indicated a location bias in signaling, whereby cAMP generated intracellularly is more effective at propagating PKA dependent signaling than cAMP originating from the plasma membrane (*4*, *11–13*, *32*, *36–39*). Given the compartmentalized nature of cAMP signaling, it is thought that moving cAMP sources away from high phosphodiesterase activity at the plasma membrane and toward nuclear and perinuclear stores of PKA promotes more efficient cAMP signal transduction to the nucleus (*11–13*, *32*, *36*, *37*). Our results support this paradigm. Furthermore, our comparisons of β2AR and VIPR1 indicate that many mechanisms can underlie location bias in signaling, and the balance of endocytosis as a plasma membrane signal attenuator versus an internal signal booster contributes to signaling diversity among receptors that undergo agonist-induced trafficking.

In contrast, we found the human A_{2B}R neither detectably internalizes nor strongly desensitizes upon prolonged agonist exposure. Thus, the human A_{2B}R appears to activate the cAMP/PKA in a fully endocytosis-independent

manner, in marked contrast to VIPR1 and β2AR. We did detect some internalized $A_{2B}R$ by microscopy, but mG_s was not detectably associated. Accordingly, the simplest interpretation of our results is that downstream responses—including nuclear PKA activity and robust transcriptional activation—can be instigated from sustained plasma membrane-derived signaling, circumventing the aforementioned endosomal spatial bias for these processes.

Based on these results, we propose a simple model for encoding the selectivity of signaling through the cAMP pathway that uses the location and duration of signal initiation as independent variables (Figure 7). VIP and Iso limit signaling from the plasma membrane by desensitization and use endocytosis to drive signaling to the nucleus through location bias. NECA drives downstream signaling primarily through its failure to desensitize in the plasma membrane, producing a prolonged elevation of global cAMP irrespective of endocytosis.

We were surprised that NECA stimulated stronger CREB phosphorylation and transcriptional activation than Iso (Figure 6A, Supplementary Figure 10) despite the two eliciting comparable levels of nuclear PKA activity (Figure 2C, Supplementary Figure 5A-B). One potential explanation for this observation could be that $A_{2B}R$ is activating additional signaling pathways. CREB can also be phosphorylated by other kinases, including mitogen-activated protein kinases (MAPKs) and Ca^{2+}/calmodulin-dependent protein kinases (CaMKs) (*40*), and $A_{2B}R$ has been shown to also couple to Gq, which raises intracellular calcium levels (*41*). Thus, while our results establish a clear role for trafficking in functional ligand discrimination, this mechanism works in concert with other parameters to maintain signaling compartmentalization and encode downstream specificity (*42*, *43*). As an example, we note that the responses among all three receptors became more similar at sub-saturating agonist concentrations (Supplementary Figure 4A-C), highlighting the importance of agonist treatment regimes. In addition to concentration, the duration of stimulation is also likely critical for ligand discrimination, particularly for GPCRs like $A_{2B}R$ that are not afforded protection from ligand washout by endocytosis (*44*, *45*).

In summary, we show that endocytosis indeed sculpts the cellular signaling profiles of ligands sensed by the natively expressed cellular GPCR repertoire. These ligands produce a range of signaling profiles that are determined by GPCR-specific differences in desensitization and endocytosis as independent variables. Our results support the evolving view of compartmentalized GPCR-mediated cAMP signaling (*8*) and suggest that receptor trafficking dynamics can finely tune downstream responses to GPCRs that share common signal transduction networks.

Materials and Methods

Cell Culture

HEK293 cells (ATCC CRL1573) were cultured in DMEM (Gibco 1196511) supplemented with 10% FBS (Hyclone SH30910.03 or R&D Systems S12495 via UCSF Tissue Culture Facility) and grown at 37 °C with 5% CO_2. Halo-β2AR and inducible Halo-VIPR1 stable cell lines have been previously described (*20*). Cells stably expressing Halo-$A_{2B}R$ were selected with 25 µg/mL zeocin, and cells stably expressing FLAG-β2AR or FLAG-$A_{2B}R$ were selected with 500 µg/mL geneticin.

CRISPR knockout of $A_{2B}R$

Cells were electroporated with single guide RNAs ($A_{2B}R$: GACACAGGACGCGCTGTACG, NT: GCACUACCAGAGCUAA; Synthego) in complex with Cas9 (UC Berkeley Macrolab) before monoclonal selection. Genetic modifications were verified by Sanger sequencing of PCR amplicons (primers: TGCGTGAGCACCAGCACGAA and GGCAATTTGTTAGTTATCCGCCGC).

Reagents and antibodies
Information about the chemicals and antibodies used in this study can be found in Supplementary Tables 4 and 5.

DNA Constructs and BacMam virus
Details about the plasmids and BacMam viruses used in this study can be found in Supplementary Table 6. Transfections using Lipofectamine 2000 (ThermoFisher) were carried out 24-48 hours before experiments according to the manufacturer's protocol. BacMam viruses from pCMV-Dest plasmids were produced according to the manufacturer's protocol (Invitrogen) and added to cells 24 hours before experiments.

Fluorescent biosensor assays
Cells treated with cADDis (Montana Molecular #U0200G), ExRai-AKAR2, mCherry, and/or mCherry-DynK44E BacMams were plated into 96-well plates (Corning 3340) coated with poly-L-lysine (Millipore Sigma P8920). After 24 h, cells were washed twice with assay buffer (20 mM HEPES pH 7.4, 135 mM NaCl, 5 mM KCl, 0.4 mM $MgCl_2$, 1.8 mM $CaCl_2$, 5 mM d-glucose) before a 10-min incubation in a prewarmed 37 °C plate reader (Spark, Tecan Life Sciences, controlled by SparkControl v3.2). When appropriate, 30 μM Dyngo4a or vehicle was added immediately prior to preincubation. For βAR antagonist experiments, cells were preincubated for 30 minutes in assay buffer containing antagonist (300 nM GCP 20712, 300 nM ICI 118551, or 10 μM Alp) or vehicle.

For cADDis, fluorescence was read at an excitation wavelength of 500/5 nm and an emission wavelength of 530/10 nm. For ExRai-AKAR2, fluorescence was read using 400/20 nm and 485/20 nm excitation filters and a 520/10 nm emission filter. mCherry was read using a 560/20 nm excitation filter and a 620/10 nm emission filter. Data were collected every 30 seconds for 35 minutes, with vehicle or agonist added at 5 minutes.

Intracellular cAMP was calculated using raw fluorescence (F), while intracellular PKA activity was calculated using the ratio of fluorescence ($R = F_{485} / F_{400}$) background corrected by subtracting the average fluorescence of untransduced wells at each timepoint (*29*). Changes in cAMP ($\Delta F/F_0$) and PKA activity ($\Delta R/R_0$) were calculated as the change in fluorescence ($\Delta F = F - F_0$ or $\Delta R = R - R_0$) normalized to the average of the 5-min baseline (F_0 or R_0). For samples expressing mCherry or mCherry-DynK44E, curves were further normalized to the peak fluorescence change $(\Delta F/F_0)_{max}$ or $(\Delta R/R_0)_{max}$ as noted in figure legends. Difference curves were calculated by subtracting mCherry-DynK44E curves from mCherry curves. Sustained activity, measured 30 minutes post-agonist addition, was calculated as $(\Delta F/F_0)_{30} / (\Delta F/F_0)_{max} \times 100$ or $(\Delta R/R_0)_{30} / (\Delta R/R_0)_{max} \times 100$. Integrated signal was calculated as an area under the curve following agonist addition. For dose–response curves, data were fit to a three-parameter dose-response equation in Prism (v.10). When top and bottom plateaus could not be automatically fit, these were constrained to the average maximum signal and zero, respectively.

Internalization by flow cytometry
Cells stably expressing N-terminally tagged GPCRs in 12-well plates were treated with Iso (100 nM or 1 μM), 500 nM VIP, or 20 μM NECA for the indicated times. After three washes with cold PBS, cell surface receptors were labeled with 200 nM JF_{635}i-HTL (HaloTagged receptors) or M1 antibody conjugated to Alexa Fluor 647 (FLAG-tagged receptors) for 30 minutes at 4 °C. FLAG-tagged samples were mechanically lifted, while HaloTagged samples were washed once with PBS-EDTA (UCSF Cell Culture Facility) before being lifted with TrypLE Express (Thermo Fisher). Surface staining was measured on an Attune NxT Flow Cytometer equipped with a CytKick Autosampler and controlled by Attune Cytometric Software (v5.3.2415.0) using a 561 nm excitation laser and a 620/15 nm emission filter. Data were analyzed using FlowJo v.10.10.0 software (BD Life

Sciences). Populations were gated for cells expressing receptor, and internalization was calculated as [1 - (F_t / F_{t0})] * 100, where F_t is the median fluorescence at time t. Each biological replicate represents the average of three technical replicates.

Western blot

Cells plated in poly-L-lysine-coated (Millipore Sigma P8920) 6-well plates were treated with vehicle (water), 100 nM Iso, 100 nM VIP, or 100 μM NECA for 15 minutes. After three rapid washes with cold PBS, cells were lysed in RIPA (50 mM Tris pH 7.4, 150 mM NaCl, 1% Triton X-100, 0.5% SDC, 0.1% SDS), sonicated, and spun at 17,000xg for 10 minutes. Supernatant protein concentrations were normalized before SDS-PAGE and western blot analysis using the antibodies listed in Supplementary Table 5. Blots were imaged using an Odyssey Imager (v.2.0.3, LI-COR Biosciences) and quantified using Fiji (v.2.3.0) (*46*). For quantification, pCREB intensities were normalized to total CREB intensities.

RNAseq

Cells plated in 6-well plates were washed twice with DMEM before addition of agonist (100 nM Iso, 500 nM VIP, or 20 μM NECA) or their corresponding vehicles (1 μM ascorbic acid, water, or 0.05% DMSO) diluted in DMEM. After a 90 minute incubation at 37 °C with 5% CO_2, cells were washed once with cold PBS and stored at -70 °C. RNA was extracted using the RNeasy Mini Kit (Qiagen) and further purified using the RNA Clean & Concentrator kit (Zymo Research). Barcoded 3'Tag-Seq libraries were prepared using the QuantSeq FWD kit (Lexogen, Vienna, Austria) for multiplexed sequencing according to the recommendations of the manufacturer. The fragment size distribution of the libraries was verified via micro-capillary gel electrophoresis on a Bioanalyzer 2100 (Agilent, Santa Clara, CA). The libraries were quantified by fluorometry on a Qubit instrument (LifeTechnologies, Carlsbad, CA) and pooled in equimolar ratios. Eighteen libraries were sequenced on one lane of an HiSeq4000 sequencer (Illumina, San Diego, CA) with single-end 100 bp reads. The sequencing generated more than 4 million reads per library. Raw reads were preprocessed using HTStream, version 1.3.3 (https://s4hts.github.io/HTStream/) and aligned to GRCh38 using STAR, version 2.7.9a (*47*). Differential expression analyses were conducted using limma-voom (*48*) (limma version 3.50.0, edgeR version 3.36.0), in R version 4.1.0 (https://www.R-project.org/).

Luminescence transcriptional reporter assay

Cells were transfected with pGL4.29[luc2P/CRE/Hygro] (Promega E8471) and replated into white 96-well plates (Corning 3917) coated with poly-L-lysine (Millipore Sigma P8920) at a concentration of 50,000 cells/well. If cells were pretreated with mCherry or mCherry-DynK44E, BacMam virus was added upon replating. After overnight incubation, media was replaced before treatment with vehicle (water or DMSO), Iso, VIP, or NECA at the indicated concentrations. Cells were incubated at 37 °C with 5% CO_2 for 4.75 hours followed by a 15 minute incubation at room temperature. After a wash with room temperature assay buffer (20 mM HEPES pH 7.4, 135 mM NaCl, 5 mM KCl, 0.4 mM $MgCl_2$, 1.8 mM $CaCl_2$, 5 mM d-glucose), cells were treated with 1.6 mM D-luciferin (Gold Biotechnology LUCNA) in assay buffer. Luminescence was read two minutes later by plate reader (Spark, Tecan Life Sciences, controlled by SparkControl v3.2). Change in luminescence (ΔLum) was calculated as the ratio of the average luminescence of agonist-treated wells divided by the average luminescence of vehicle-treated wells. Within each biological replicate, changes in luminescence were normalized to either a 10 μM forskolin control or each agonist's maximum response in the mCherry control.

Live-cell imaging

Cells were cotransfected with FLAG-tagged GPCRs and venus-mini-G_s and replated into poly-L-lysine (Millipore Sigma P8920) coated glass bottom dishes (Cellvis D35-20-1.5-N). After 48 hours, cells were labeled with M1 antibody conjugated to Alexa Fluor 647 for 10 minutes at 37 °C, washed three times, and imaged live in DMEM

without phenol red (Gibco 31053028) supplemented with 30 mM HEPES pH 7.4. Confocal microscopy was carried out on Nikon Ti inverted microscope controlled by NIS Elements HC v.5.20.02 (Nikon) and fitted with a CSU-22 spinning disk unit (Yokogawa), custom laser launch (100 mW at 405, 488, 561 and 640 nm, Coherent OBIS), Sutter emission filter wheel, an Apo TIRF ×100/1.49 numerical aperture oil objective (Nikon), and a Photometrics Evolve Delta EMCCD camera. Cells were kept in a temperature- and humidity-controlled chamber (Okolab) at 37 °C. Cells were imaged for 2 minutes before addition of agonist and 20 minutes after agonist. Images were processed and analyzed using Fiji (v.2.3.0) (*40*).

Data analysis and reproducibility

Statistical analysis and curve fitting was carried out using Prism (v.10, GraphPad) as noted in figure legends. All data are shown as individual biological replicates or as mean ± standard deviation from at least three biologically independent experiments, unless otherwise noted. For fluorescent biosensor assays, luminescent transcriptional reporter assays, and flow cytometry internalization assays, each biological replicate represents the average of at least two technical replicates.

References

1. K. L. Pierce, R. T. Premont, R. J. Lefkowitz, Seven-transmembrane receptors. *Nat. Rev. Mol. Cell Biol.* **3**, 639–650 (2002).
2. S. J. Smith, M. von Zastrow, A Molecular Landscape of Mouse Hippocampal Neuromodulation. *Front. Neural Circuits* **16**, 836930 (2022).
3. E. Hu, L. Demmou, B. Cauli, T. Gallopin, H. Geoffroy, R. M. Harris-Warrick, D. Paupardin-Tritsch, B. Lambolez, P. Vincent, R. Hepp, VIP, CRF, and PACAP Act at Distinct Receptors to Elicit Different cAMP/PKA Dynamics in the Neocortex. *Cereb. Cortex* **21**, 708–718 (2011).
4. N.-N. Aye-Han, M. D. Allen, Q. Ni, J. Zhang, Parallel tracking of cAMP and PKA signaling dynamics in living cells with FRET-based fluorescent biosensors. *Mol. Biosyst.* **8**, 1435 (2012).
5. Y. Manchanda, S. Bitsi, S. Chen, J. Broichhagen, J. Bernardino De La Serna, B. Jones, A. Tomas, Enhanced Endosomal Signaling and Desensitization of GLP-1R vs GIPR in Pancreatic Beta Cells. *Endocrinology* **164**, bqad028 (2023).
6. J. S. Hayes, L. L. Brunton, J. H. Brown, J. B. Reese, S. E. Mayer, Hormonally specific expression of cardiac protein kinase activity. *Proc. Natl. Acad. Sci.* **76**, 1570–1574 (1979).
7. M. J. Lohse, A. Bock, M. Zaccolo, G Protein–Coupled Receptor Signaling: New Insights Define Cellular Nanodomains. *Annu. Rev. Pharmacol. Toxicol.* **64**, 387–415 (2024).
8. D. Calebiro, T. Miljus, S. O'Brien, Endomembrane GPCR signaling: 15 years on, the quest continues. *Trends Biochem. Sci.* **50**, 46–60 (2025).
9. S. S. Taylor, P. Zhang, J. M. Steichen, M. M. Keshwani, A. P. Kornev, PKA: Lessons learned after twenty years. *Biochim. Biophys. Acta BBA - Proteins Proteomics* **1834**, 1271–1278 (2013).
10. A. Bock, R. Irannejad, J. D. Scott, cAMP signaling: a remarkably regional affair. *Trends Biochem. Sci.* **49**, 305–317 (2024).
11. A. Godbole, S. Lyga, M. J. Lohse, D. Calebiro, Internalized TSH receptors en route to the TGN induce local Gs-protein signaling and gene transcription. *Nat. Commun.* **8** (2017).
12. N. G. Tsvetanova, M. von Zastrow, Spatial encoding of cyclic AMP signaling specificity by GPCR endocytosis. *Nat. Chem. Biol.* **10**, 1061–1065 (2014).
13. N. G. Tsvetanova, M. Trester-Zedlitz, B. W. Newton, G. E. Peng, J. R. Johnson, D. Jimenez-Morales, A. P. Kurland, N. J. Krogan, M. Von Zastrow, Endosomal cAMP production broadly impacts the cellular phosphoproteome. *J. Biol. Chem.* **297**, 100907 (2021).
14. A. D. White, K. A. Peña, L. J. Clark, C. S. Maria, S. Liu, F. G. Jean-Alphonse, J. Y. Lee, S. Lei, Z. Cheng, C.-L. Tu, F. Fang, N. Szeto, T. J. Gardella, K. Xiao, S. H. Gellman, I. Bahar, I. Sutkeviciute, W. Chang, J.-P. Vilardaga, Spatial bias in cAMP generation determines biological responses to PTH type 1 receptor activation. *Sci. Signal.* **14**, eabc5944 (2021).
15. A. C. Hanyaloglu, M. von Zastrow, Regulation of GPCRs by Endocytic Membrane Trafficking and Its Potential Implications. *Annu. Rev. Pharmacol. Toxicol.* **48**, 537–568 (2008).

16. E. V. Moo, J. R. van Senten, H. Bräuner-Osborne, T. C. Møller, Arrestin-Dependent and -Independent Internalization of G Protein–Coupled Receptors: Methods, Mechanisms, and Implications on Cell Signaling. *Mol. Pharmacol.* **99**, 242–255 (2021).
17. M. Zeghal, G. Laroche, J. D. Freitas, R. Wang, P. M. Giguère, Profiling of basal and ligand-dependent GPCR activities by means of a polyvalent cell-based high-throughput platform. *Nat. Commun.* **14**, 3684 (2023).
18. M. A. Shetzline, J. K. L. Walker, K. J. Valenzano, R. T. Premont, Vasoactive Intestinal Polypeptide Type-1 Receptor Regulation. *J. Biol. Chem.* **277**, 25519–25526 (2002).
19. J. Cooper, S. J. Hill, S. P. H. Alexander, An endogenous A_{2B} adenosine receptor coupled to cyclic AMP generation in human embryonic kidney (HEK 293) cells. *Br. J. Pharmacol.* **122**, 546–550 (1997).
20. E. E. Blythe, M. Von Zastrow, β-Arrestin-independent endosomal cAMP signaling by a polypeptide hormone GPCR. *Nat. Chem. Biol.* **20**, 323–332 (2024).
21. V. Burghi, J. S. Paradis, A. Officer, S. R. Adame-Garcia, X. Wu, E. S. F. Matthees, B. Barsi-Rhyne, D. J. Ramms, L. Clubb, M. Acosta, P. Tamayo, M. Bouvier, A. Inoue, M. Von Zastrow, C. Hoffmann, J. S. Gutkind, Gαs is dispensable for β-arrestin coupling but dictates GRK selectivity and is predominant for gene expression regulation by β2-adrenergic receptor. *J. Biol. Chem.* **299**, 105293 (2023).
22. J. G. Baker, The selectivity of *β* -adrenoceptor antagonists at the human *β* 1, *β* 2 and *β* 3 adrenoceptors. *Br. J. Pharmacol.* **144**, 317–322 (2005).
23. C. T. H. Jonker, C. Deo, P. J. Zager, A. N. Tkachuk, A. M. Weinstein, E. Rodriguez-Boulan, L. D. Lavis, R. Schreiner, Accurate measurement of fast endocytic recycling kinetics in real time. *J. Cell Sci.* **133**, jcs.231225 (2020).
24. M. Von Zastrow, B. K. Kobilka, Ligand-regulated internalization and recycling of human beta 2-adrenergic receptors between the plasma membrane and endosomes containing transferrin receptors. *J. Biol. Chem.* **267**, 3530–3538 (1992).
25. S. J. Mundell, A.-L. Matharu, E. Kelly, J. L. Benovic, Arrestin Isoforms Dictate Differential Kinetics of A2B Adenosine Receptor Trafficking. *Biochemistry* **39**, 12828–12836 (2000).
26. R. Irannejad, J. C. Tomshine, J. R. Tomshine, M. Chevalier, J. P. Mahoney, J. Steyaert, S. G. F. Rasmussen, R. K. Sunahara, H. El-Samad, B. Huang, M. von Zastrow, Conformational biosensors reveal GPCR signalling from endosomes. *Nature* **495**, 534–538 (2013).
27. B. Carpenter, C. G. Tate, Engineering a minimal G protein to facilitate crystallisation of G protein-coupled receptors in their active conformation. *Protein Eng. Des. Sel.* **29**, 583–594 (2016).
28. Q. Wan, N. Okashah, A. Inoue, R. Nehmé, B. Carpenter, C. G. Tate, N. A. Lambert, Mini G protein probes for active G protein–coupled receptors (GPCRs) in live cells. *J. Biol. Chem.* **293**, 7466–7473 (2018).
29. J.-F. Zhang, B. Liu, I. Hong, A. Mo, R. H. Roth, B. Tenner, W. Lin, J. Z. Zhang, R. S. Molina, M. Drobizhev, T. E. Hughes, L. Tian, R. L. Huganir, S. Mehta, J. Zhang, An ultrasensitive biosensor for high-resolution kinase activity imaging in awake mice. *Nat. Chem. Biol.* **17**, 39–46 (2021).
30. J. Keyes, A. Ganesan, O. Molinar-Inglis, A. Hamidzadeh, J. Zhang, M. Ling, J. Trejo, A. Levchenko, J. Zhang, Signaling diversity enabled by Rap1-regulated plasma membrane ERK with distinct temporal dynamics. *eLife* **9**, e57410 (2020).
31. N. Gervasi, R. Hepp, L. Tricoire, J. Zhang, B. Lambolez, D. Paupardin-Tritsch, P. Vincent, Dynamics of Protein Kinase A Signaling at the Membrane, in the Cytosol, and in the Nucleus of Neurons in Mouse Brain Slices. *J. Neurosci.* **27**, 2744–2750 (2007).
32. V. Sample, L. M. DiPilato, J. H. Yang, Q. Ni, J. J. Saucerman, J. Zhang, Regulation of nuclear PKA revealed by spatiotemporal manipulation of cyclic AMP. *Nat. Chem. Biol.* **8**, 375–382 (2012).
33. Z. Haj Slimane, I. Bedioune, P. Lechêne, A. Varin, F. Lefebvre, P. Mateo, V. Domergue-Dupont, M. Dewenter, W. Richter, M. Conti, A. El-Armouche, J. Zhang, R. Fischmeister, G. Vandecasteele, Control of cytoplasmic and nuclear protein kinase A by phosphodiesterases and phosphatases in cardiac myocytes. *Cardiovasc. Res.* **102**, 97–106 (2014).
34. J. H. Yang, R. K. Polanowska-Grabowska, J. S. Smith, C. W. Shields, J. J. Saucerman, PKA catalytic subunit compartmentation regulates contractile and hypertrophic responses to β-adrenergic signaling. *J. Mol. Cell. Cardiol.* **66**, 83–93 (2014).
35. J. Zhang, S. S. G. Ferguson, L. S. Barak, L. Ménard, M. G. Caron, Dynamin and β-Arrestin Reveal Distinct Mechanisms for G Protein-coupled Receptor Internalization. *J. Biol. Chem.* **271**, 18302–18305 (1996).

36. G. E. Peng, V. Pessino, B. Huang, M. Von Zastrow, Spatial decoding of endosomal cAMP signals by a metastable cytoplasmic PKA network. *Nat. Chem. Biol.* **17**, 558–566 (2021).
37. B. K. A. Willette, J.-F. Zhang, J. Zhang, N. G. Tsvetanova, Endosome positioning coordinates spatially selective GPCR signaling. *Nat. Chem. Biol.* **20**, 151–161 (2024).
38. C. P. O'Banion, B. M. Vickerman, L. Haar, D. S. Lawrence, Compartmentalized cAMP Generation by Engineered Photoactivated Adenylyl Cyclases. *Cell Chem. Biol.* **26**, 1393-1406.e7 (2019).
39. L. Ripoll, Y. Li, C. W. Dessauer, M. Von Zastrow, Spatial organization of adenylyl cyclase and its impact on dopamine signaling in neurons. *Nat. Commun.* **15**, 8297 (2024).
40. A. J. Shaywitz, M. E. Greenberg, CREB: A Stimulus-Induced Transcription Factor Activated by A Diverse Array of Extracellular Signals. *Annu. Rev. Biochem.* **68**, 821–861 (1999).
41. Z.-G. Gao, A. Inoue, K. A. Jacobson, On the G protein-coupling selectivity of the native A2B adenosine receptor. *Biochem. Pharmacol.* **151**, 201–213 (2018).
42. I. Masuho, R. Kise, P. Gainza, E. Von Moo, X. Li, R. Tany, H. Wakasugi-Masuho, B. E. Correia, K. A. Martemyanov, Rules and mechanisms governing G protein coupling selectivity of GPCRs. *Cell Rep.* **42**, 113173 (2023).
43. M. Zaccolo, A. Zerio, M. J. Lobo, Subcellular Organization of the cAMP Signaling Pathway. *Pharmacol. Rev.* **73**, 278–309 (2021).
44. S. Ferrandon, T. N. Feinstein, M. Castro, B. Wang, R. Bouley, J. T. Potts, T. J. Gardella, J.-P. Vilardaga, Sustained cyclic AMP production by parathyroid hormone receptor endocytosis. *Nat. Chem. Biol.* **5**, 734–742 (2009).
45. D. Calebiro, V. O. Nikolaev, M. C. Gagliani, T. de Filippis, C. Dees, C. Tacchetti, L. Persani, M. J. Lohse, Persistent cAMP-Signals Triggered by Internalized G-Protein–Coupled Receptors. *PLoS Biol.* **7**, e1000172 (2009).
46. J. Schindelin, I. Arganda-Carreras, E. Frise, V. Kaynig, M. Longair, T. Pietzsch, S. Preibisch, C. Rueden, S. Saalfeld, B. Schmid, J.-Y. Tinevez, D. J. White, V. Hartenstein, K. Eliceiri, P. Tomancak, A. Cardona, Fiji: an open-source platform for biological-image analysis. *Nat. Methods* **9**, 676–682 (2012).
47. A. Dobin, C. A. Davis, F. Schlesinger, J. Drenkow, C. Zaleski, S. Jha, P. Batut, M. Chaisson, T. R. Gingeras, STAR: ultrafast universal RNA-seq aligner. *Bioinforma. Oxf. Engl.* **29**, 15–21 (2013).
48. M. E. Ritchie, B. Phipson, D. Wu, Y. Hu, C. W. Law, W. Shi, G. K. Smyth, limma powers differential expression analyses for RNA-sequencing and microarray studies. *Nucleic Acids Res.* **43**, e47–e47 (2015).
49. M.J. Klauer, K.L. Hall, C. A. D. Jagla, N. G. Tsvetanova, Extensive location bias of the GPCR-dependent translatome via site-selective activation of mTOR. *Proc. Natl. Acad. Sci.* **122**, e2414738122 (2025).
50. X. Zhang, et al., Genome-wide analysis of cAMP-response element binding protein occupancy, phosphorylation, and target gene activation in human tissues. *Proc. Natl. Acad. Sci.* **102**, 4459-4464 (2005).
51. T. T. Cao, H. W. Deacon, D. Deczek, A. Bretscher, M. Von Zastrow, A kinase-regulated PDZ-domain interaction controls endocytic sorting of the b2-adrenergic receptor. *Nature* **401**, 286-290 (1999).

Acknowledgements

We thank Jin Zhang and Luke Lavis for generously sharing reagents, Nicole Fisher for assistance with cloning and viral production, Andy Zhou for assistance with data visualization, the von Zastrow lab for helpful discussion, and the following core facilities for providing services to support this research: the UCSF Center for Advanced Light microscopy (Nico Sturrman, Kari Herrington, Micaela Lasser, DeLaine Larsen, and SoYeon Kim) and the UCSF Helen Diller Family Comprehensive Cancer Center Laboratory for Cell Analysis (Sarah Elmes; supported by NIH under award P30CA082103). The library preparation and sequencing was carried out at the DNA Technologies and Expression Analysis Cores at the UC Davis Genome Center, supported by NIH Shared Instrumentation Grant 1S10OD010786-01, and DGE analysis was carried out at the Bioinformatics Core at the UC Davis Genome Center.

Funding
This work was supported by the National Institutes of Health National Institute on Drug Abuse (R01DA010711 and R01DA012864 to M.v.Z.). E.E.B. was supported by an NIH/NRSA Postdoctoral Fellowship (F32CA260118) and a K99 (K99GM151441). R.R.F. is supported by a NIH/NRSA Postdoctoral Fellowship (1F32MH130096).

Author Contributions
E.E.B. and M.v.Z. conceived of the study. E.E.B., R.R.F., and M.v.Z. designed experiments. E.E.B. and R.R.F. carried out experiments. E.E.B., R.R.F., and M.v.Z. analyzed data and wrote the manuscript.

Competing Interests
The authors declare no competing interests.

Data and Materials Availability
RNAseq data is available in the Gene Expression Omnibus repository (GSE290019). Other data and materials are available upon request.

Figures

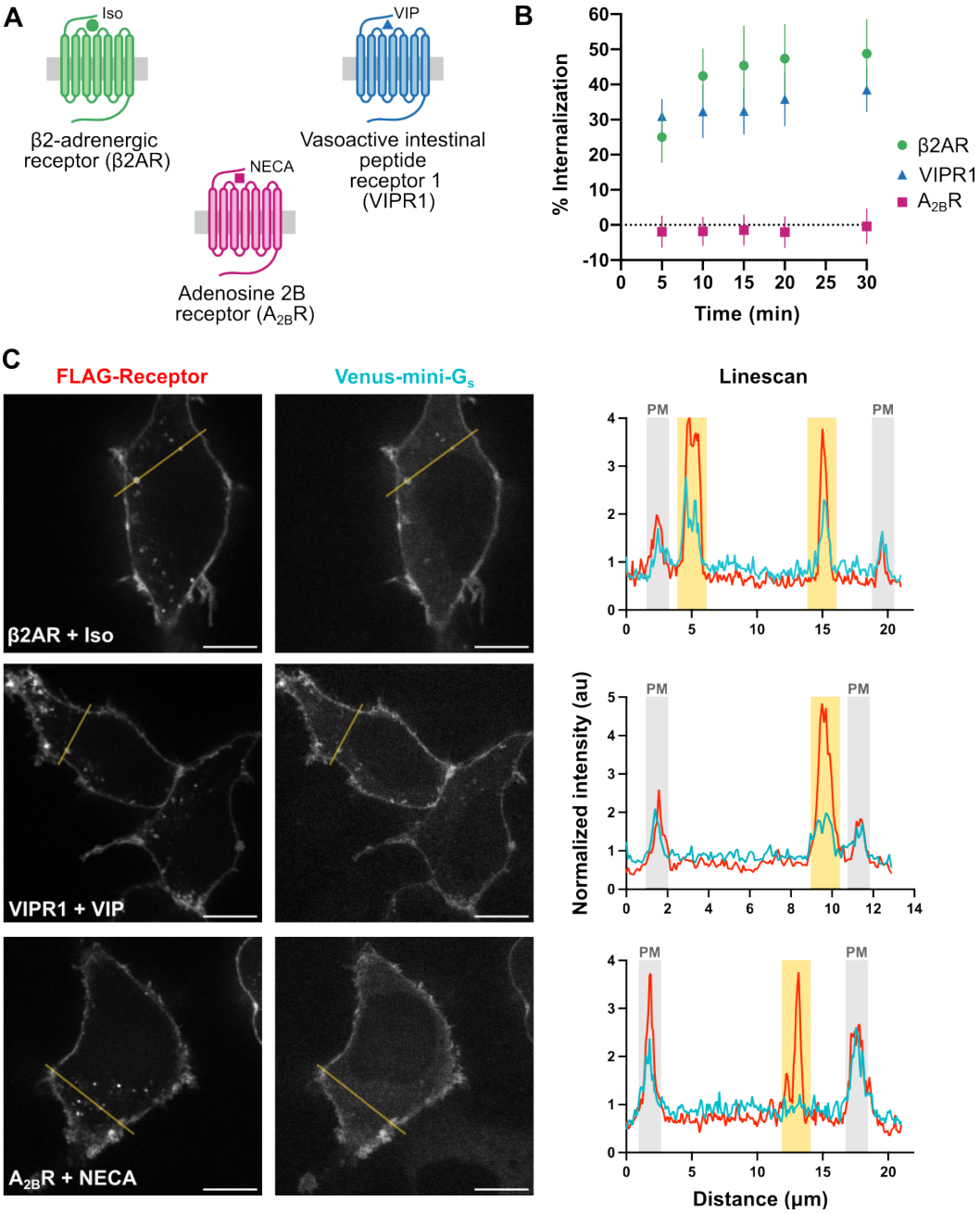

Figure 1. $A_{2B}R$ does not undergo appreciable agonist-induced endocytosis. (A) Three endogenously coexpressed GPCRs and their agonists used in this study. (B) Time course of agonist-induced internalization of HaloTagged GPCRs, as measured by flow cytometry. Receptors were stimulated with agonist (1 μM Iso, 500 nM VIP, or 20 μM NECA) for the noted times, and receptors remaining on the surface were labeled with a cell-impermeant HaloTag dye. N = 3 independent experiments, and error bars = S.D. (C) Colocalization of FLAG-tagged GPCRs and venus-mini-G_s 20 minutes after stimulation with agonist (1 μM Iso, 500 nM VIP, or 20 μM NECA). Prior to agonist stimulation, cells were treated with M1 anti-FLAG antibody labeled with Alexa Fluor 647. Scale bar is 10 μm. Linescans were normalized to the average intensity in each channel, with plasma membrane (grey) and receptor puncta (yellow) indicated. Representative images from N = 3 independent experiments.

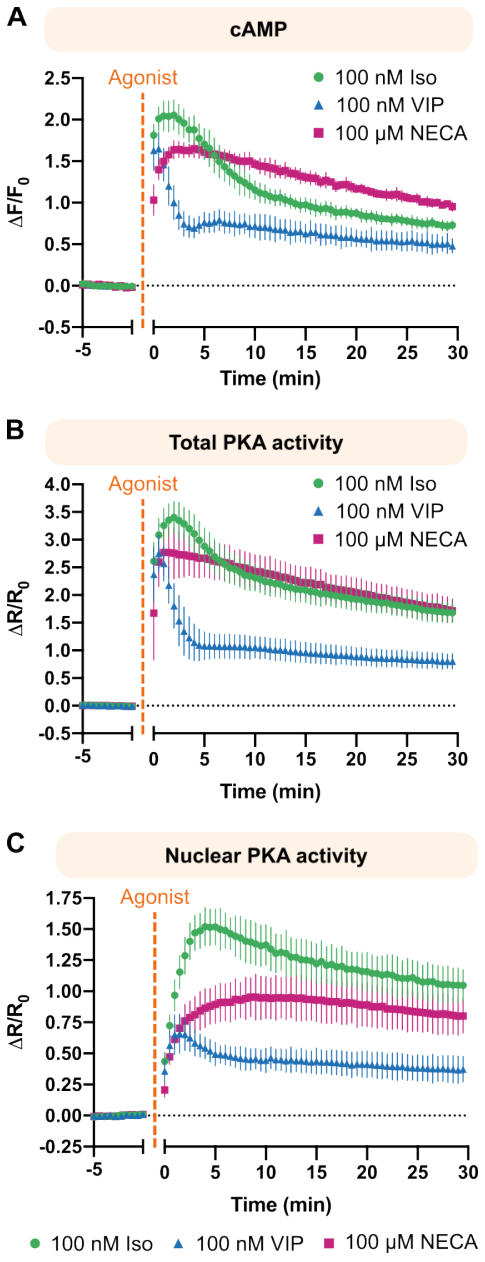

Figure 2. Endogenous GPCRs display unique cAMP and PKA signaling dynamics. Fluorescence time courses of biosensors for total intracellular cAMP (A), total cellular PKA activity (B), and nuclear PKA activity (C) upon stimulation of HEK293 cells with 100 nM Iso (green circles), 100 nM VIP (blue triangles), or 100 μM NECA (pink squares). N = 3 independent experiments, and error bars = S.D.

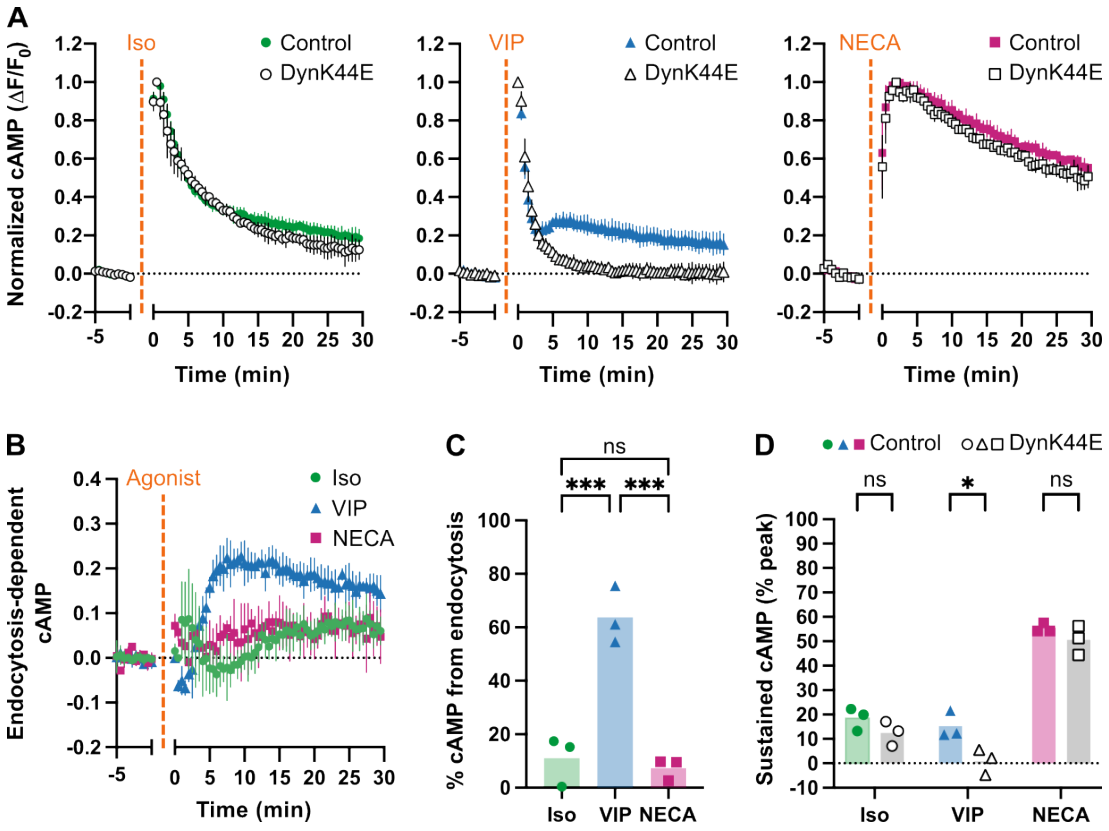

Figure 3. Endocytic inhibition halts VIP-stimulated cAMP signaling. (A) Fluorescence time course of a cAMP biosensor in cells expressing mCherry (control, colored shapes) or mCherry-DynK44E (DynK44E, open shapes) upon stimulation with 100 nM Iso (green circles), 100 nM VIP (blue triangles), or 100 μM NECA (pink squares). (B) Time course of the endocytosis-dependent fraction of cAMP responses, calculated as the difference between the control and DynK44E curves in (A). (C) Percent integrated cAMP signal that is dependent on endocytosis, calculated as the area under the difference curve in (B) normalized to the area under the corresponding control curve in (A). Significance was determined using an ordinary one-way ANOVA with Tukey's multiple comparisons test. (D) Sustained cAMP signal 30 minutes after agonist addition, calculated as the percent fluorescence at 30 minutes from the curves in (A). Significance was determined using an ordinary two-way ANOVA with Sidak's multiple comparisons test. For all panels, N = 3 independent experiments, and error bars = S.D.

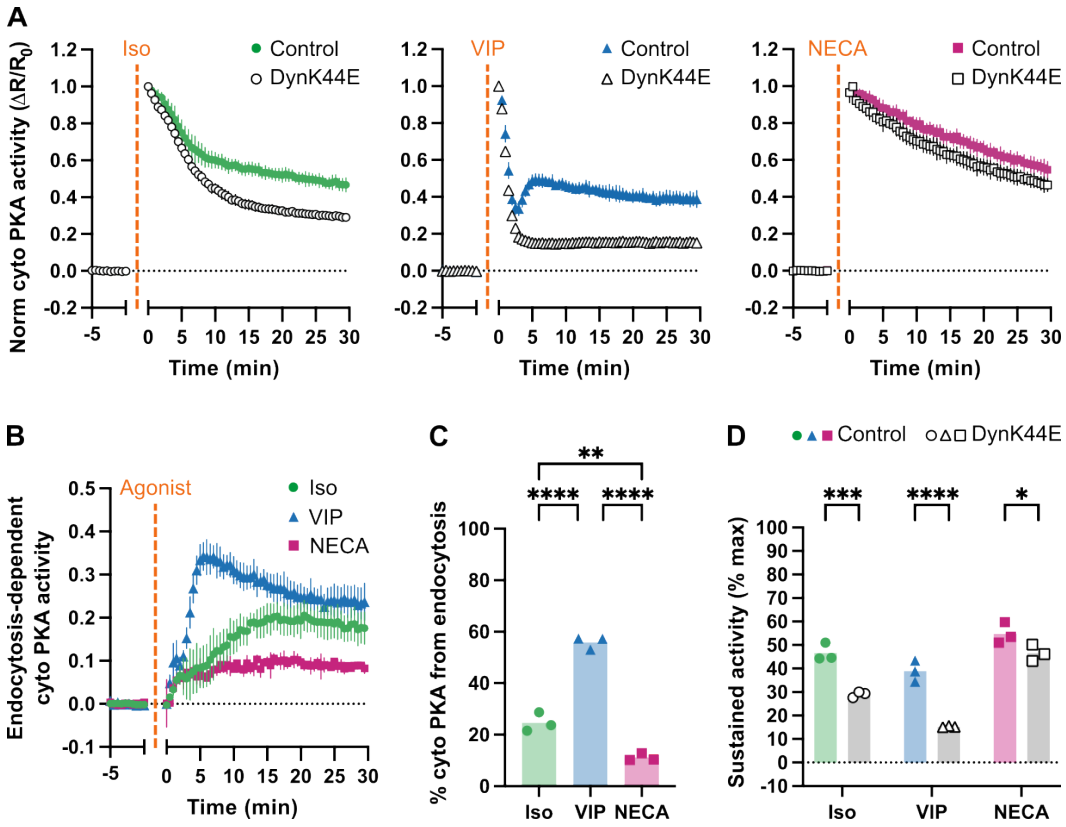

Figure 4. Endocytic inhibition dynamically blunts Iso- and VIP-stimulated cytoplasmic PKA activity. (A) Fluorescence time course of a cytoplasmic PKA activity biosensor in cells expressing mCherry (control, colored shapes) or mCherry-DynK44E (DynK44E, open shapes) upon stimulation with 100 nM Iso (green circles), 100 nM VIP (blue triangles), or 100 μM NECA (pink squares). (B) Time course of the endocytosis-dependent fraction of cytoplasmic PKA responses, calculated as the difference between the control and DynK44E curves in (A). (C) Percent integrated cytoplasmic PKA activity that is dependent on endocytosis, calculated as the area under the difference curve in (B) normalized to the area under the corresponding control curve in (A). Significance was determined using an ordinary one-way ANOVA with Tukey's multiple comparisons test. (D) Sustained cytoplasmic PKA activity 30 minutes after agonist addition, calculated as the percent fluorescence at 30 minutes from the curves in (A). Significance was determined using an ordinary two-way ANOVA with Sidak's multiple comparisons test. For all panels, N = 3 independent experiments, and error bars = S.D.

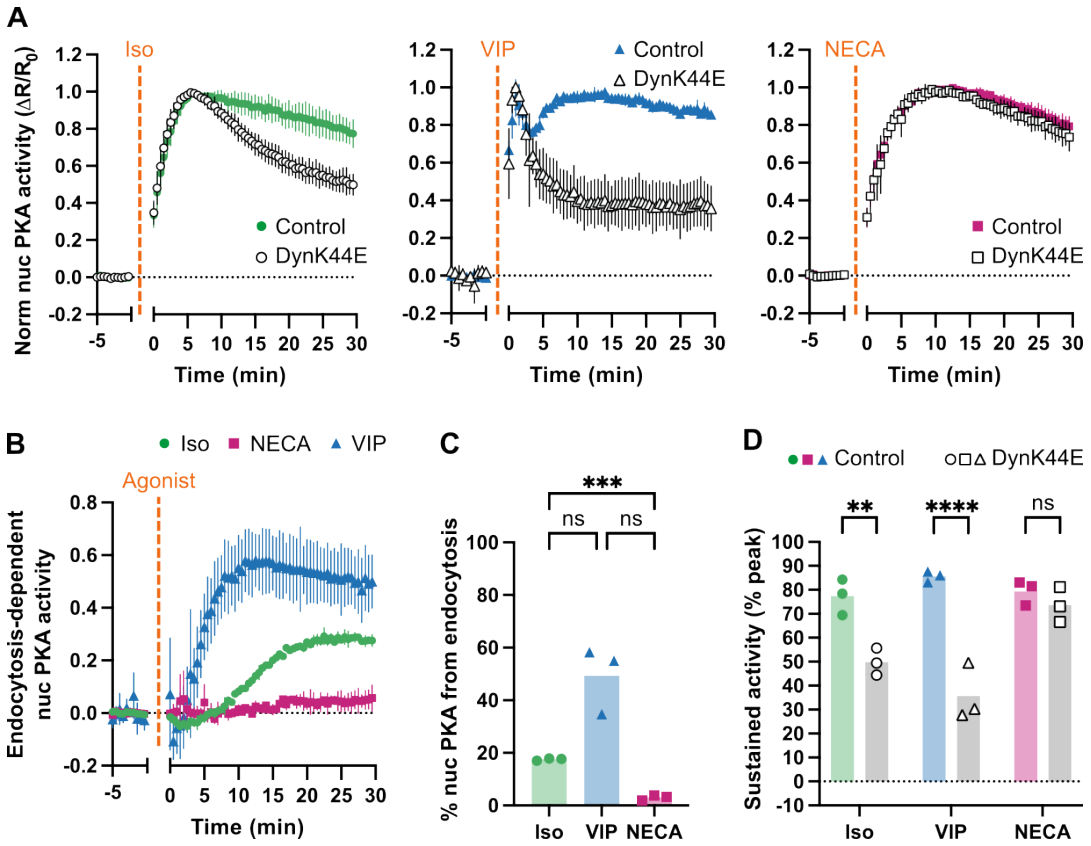

Figure 5. Only NECA can promote sustained nuclear PKA activity upon endocytic inhibition. (A) Fluorescence time course of a nuclear PKA activity biosensor in cells expressing mCherry (control, colored shapes) or mCherry-DynK44E (DynK44E, open shapes) upon stimulation with 100 nM Iso (green circles), 100 nM VIP (blue triangles), or 100 μM NECA (pink squares). (B) Time course of the endocytosis-dependent fraction of nuclear PKA response, calculated as the difference between the control and DynK44E curves in (A). (C) Percent integrated nuclear PKA activity that is dependent on endocytosis, calculated as the area under the difference curve in (B) normalized to the area under the corresponding control curve in (A). Significance was determined using a Brown-Forsythe ANOVA test with Dunnett's T3 multiple comparisons test. (D) Sustained nuclear PKA activity 30 minutes after agonist addition, calculated as the percent fluorescence at 30 minutes from the curves in (A). Significance was determined using an ordinary two-way ANOVA with Sidak's multiple comparisons test. For all panels, N = 3 independent experiments, and error bars = S.D.

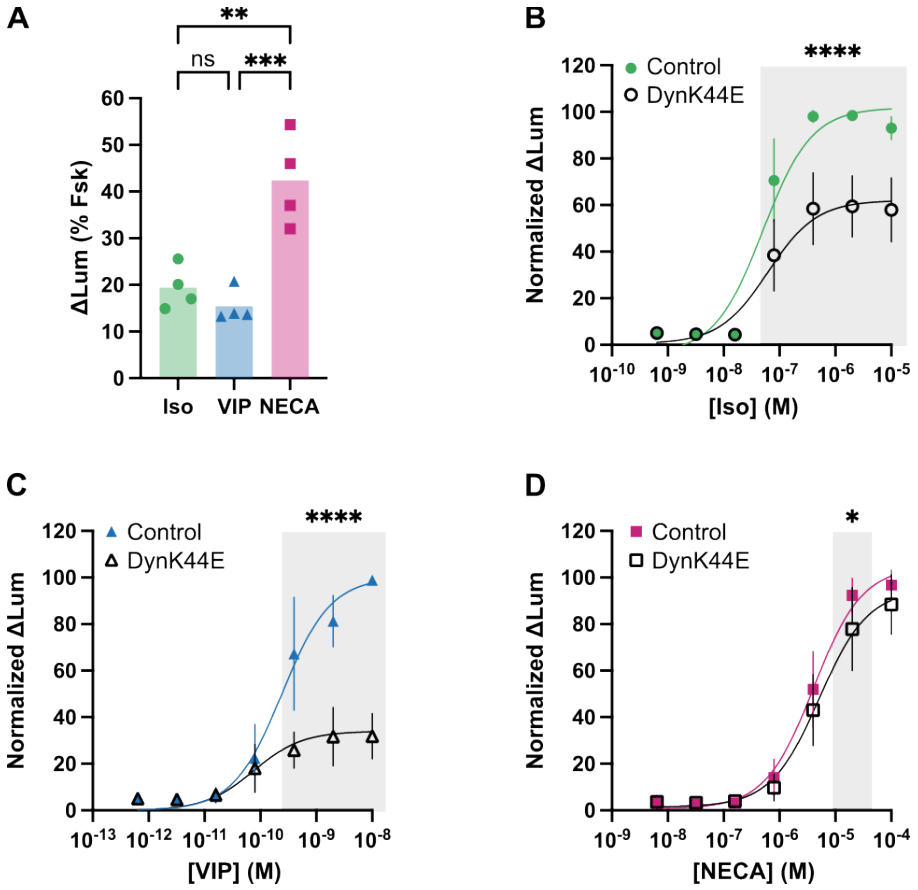

Figure 6. NECA-stimulated transcriptional activation is insensitive to endocytic inhibition. (A) Expression of CRE-luciferase transcriptional reporter upon treatment of cells with agonist (10 μM Iso, 1 μM VIP, or 100 μM NECA) for 5 hours. Change in luminescence (ΔLum) was normalized to that of a forskolin-treated control within each replicate. Significance was determined using an ordinary one-way ANOVA with Tukey's multiple comparisons test. Full dose-response curves containing these data are in Supplementary Figure 10A and Supplementary Table 1. (B-D) Transcriptional reporter assays in cells expressing mCherry (control, colored shapes) or mCherry-DynK44E (DynK44E, open shapes). Cells were treated with Iso (B), VIP (C), or NECA (D) at the indicated concentrations for 5 hours. ΔLum was normalized to the maximum control ΔLum within each replicate. Three-parameter dose-response curve fits are shown, and EC_{50}s are listed in Supplementary Table 1. Significance was determined using a two-way repeated measures ANOVA with Sidak's multiple comparisons test. For all panels, N = 4 independent experiments, and error bars = S.D.

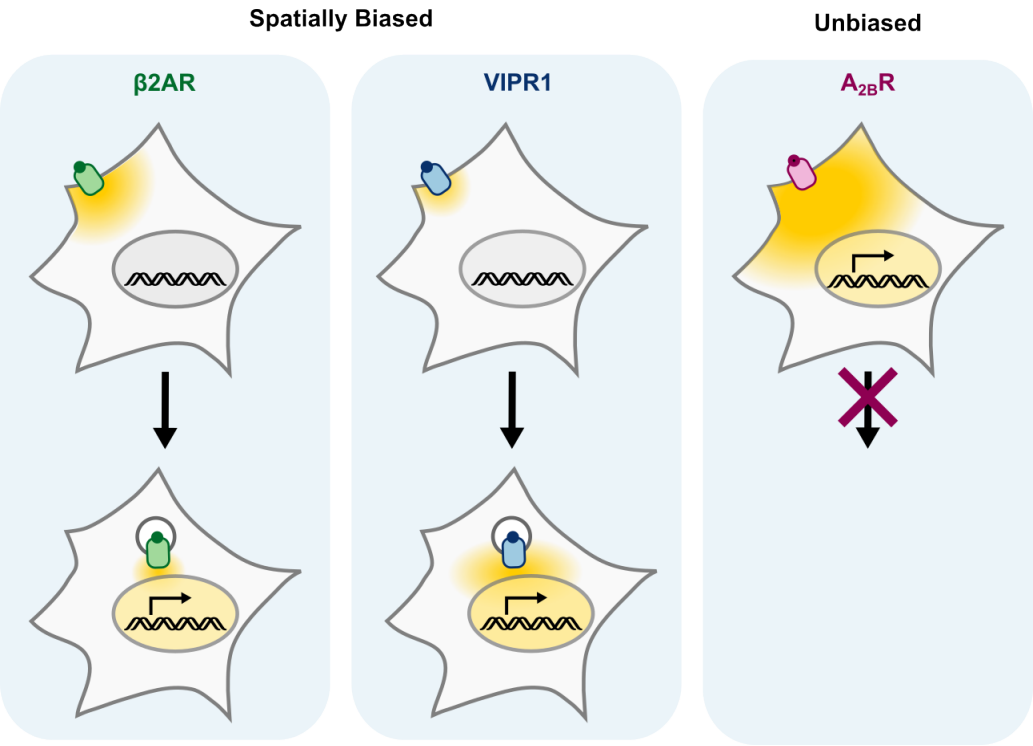

Figure 7. GPCRs employ diverse strategies to propagate signaling. For β2AR, which mediates more cAMP production (yellow) at the plasma membrane than at endosomes, receptor trafficking has little effect on overall cAMP signaling. However, receptor activity at endosomes is critical for prolonging PKA activity and for inducing a transcriptional response. For VIPR1, which mediates more cAMP production at endosomes than at the plasma membrane, receptor trafficking is necessary for prolonging both cAMP and PKA signaling and for inducing a transcriptional response. In both of these cases, sustained nuclear PKA activity and transcriptional activation are spatially biased signaling outcomes because they are promoted by receptor trafficking to and signaling from internal membranes. In contrast, $A_{2B}R$ does not undergo robust agonist-induced internalization and instead remains on the plasma membrane where it enables sustained cAMP production, prolonged PKA signaling, and transcriptional activation. Therefore, there is no spatial bias downstream of $A_{2B}R$.

Supplementary Figures

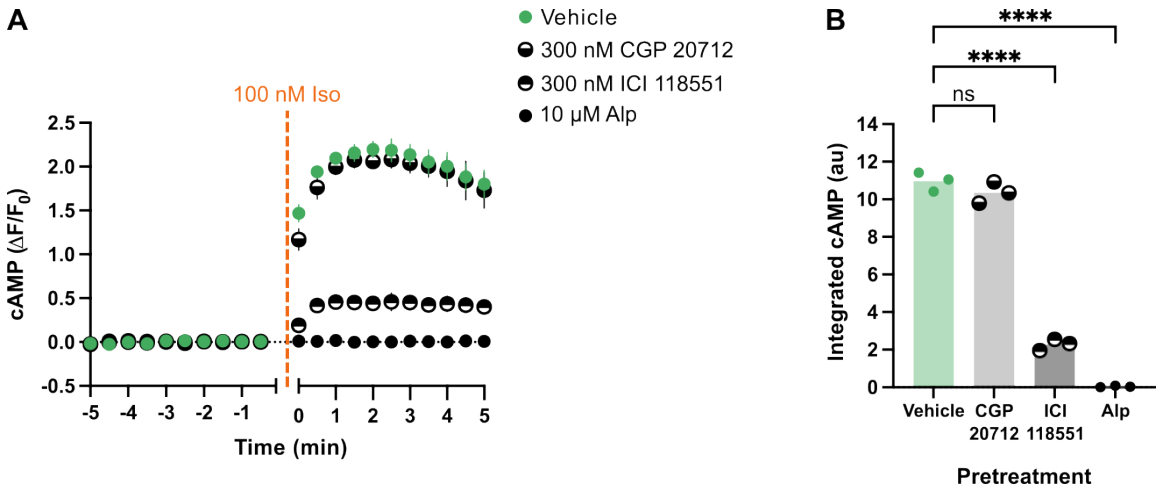

Supplementary Figure 1. β2AR is the predominant GPCR mediating Iso-stimulated cAMP activation in HEK293. (A) Iso-induced cAMP responses in HEK293 cells pretreated for 30 minutes with vehicle or βAR antagonists: 300 nM CGP 20712 (β1AR selective), 300 nM ICI 118551 (β2AR selective), or 10 μM alprenolol (Alp, non-selective). cAMP was measured by a fluorescent cAMP biosensor, and cells were stimulated with 100 nM Iso after a 5 minute baseline reading. N = 3 independent experiments, and error bars = S.D. (B) Integrated Iso-induced cAMP from (A), calculated as an area under the curve for timepoints after Iso addition. Significance was determined using an ordinary one-way ANOVA with Dunnett's multiple comparisons test.

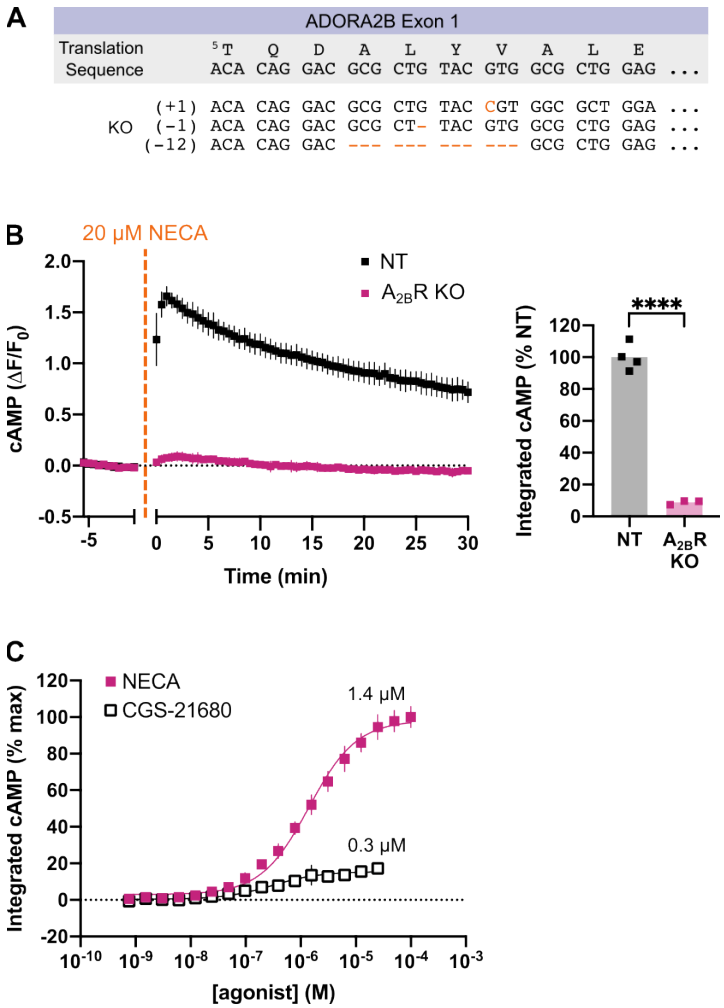

Supplementary Figure 2. $A_{2B}R$ is the primary Gs-coupled adenosine receptor subtype endogenously expressed in HEK293. (A) *ADORA2B* genetic modifications in the $A_{2B}R$ KO cell line. (B) NECA-induced cAMP responses in control (NT) or $A_{2B}R$ KO cells, as measured by a fluorescent cAMP biosensor. Integrated cAMP was calculated as an area under the curve for timepoints after NECA addition. N = 4 (NT) or N = 3 ($A_{2B}R$ KO) independent experiments. Significance was determined using an unpaired t-test. (C) Integrated cAMP responses in wild type HEK293 cells upon stimulation with NECA or the $A_{2A}R$-selective agonist CGS-21680. Data were normalized to the maximum NECA response and fit to a three-parameter dose-response curve. N = 3 independent experiments, and error bars = S.D.

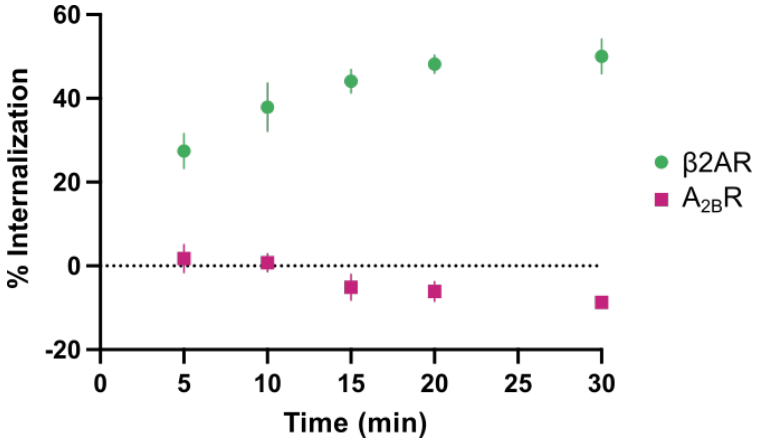

Supplementary Figure 3. FLAG-A_{2B}R does not undergo agonist-induced internalization. Time course of agonist-induced internalization of FLAG-β2AR and FLAG-A_{2B}R, as measured by flow cytometry. Receptors were stimulated with agonist (100 nM Iso or 20 μM NECA) for the noted times, and receptors remaining on the surface were labeled with M1 anti-FLAG antibody labeled with Alexa Fluor 647. N = 3 independent experiments, and error bars = S.D.

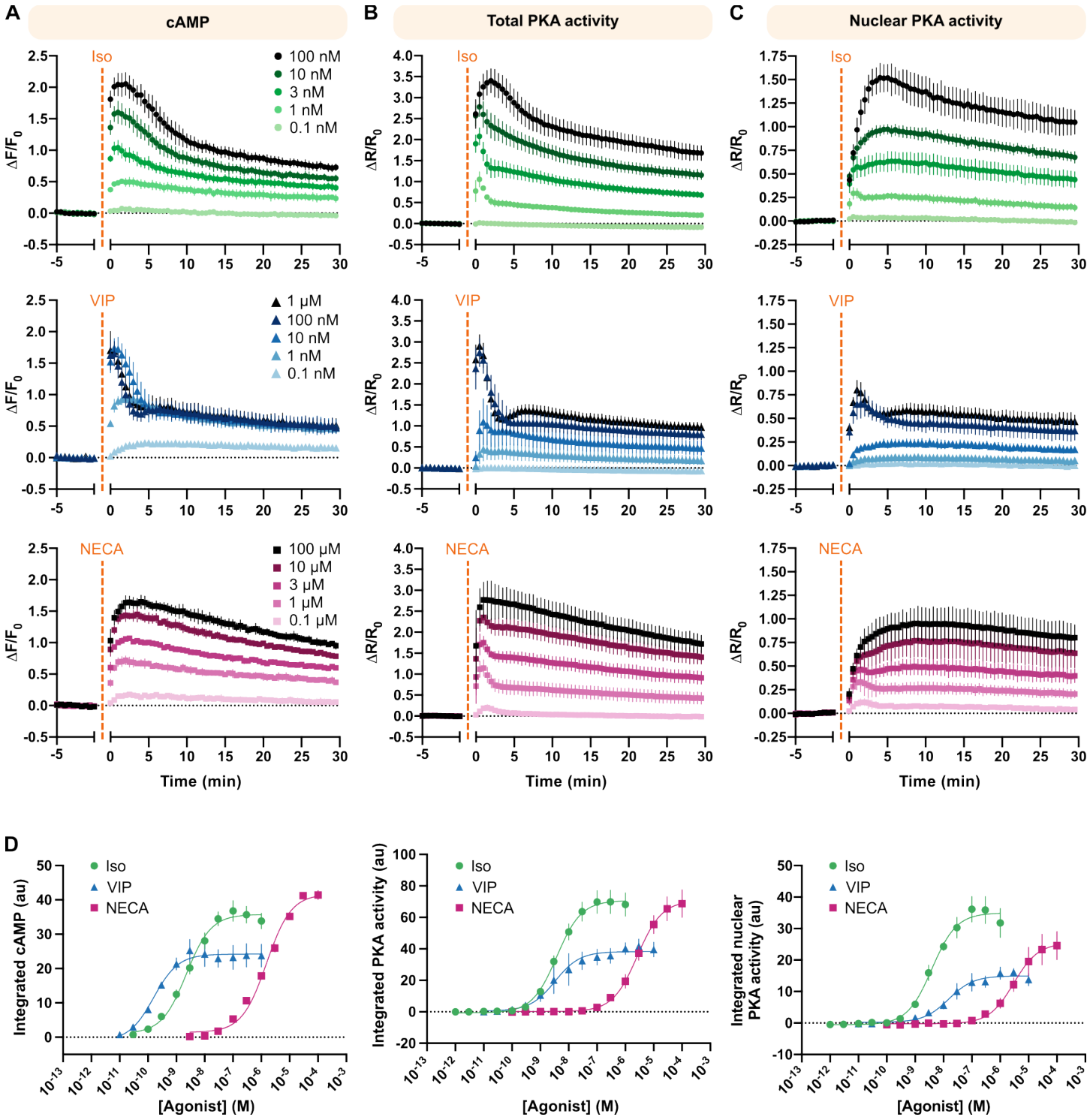

Supplementary Figure 4. Biosensor dose-response curves in HEK293 cells. (A-C) Fluorescence time courses of biosensors for total intracellular cAMP (A), total cellular PKA activity (B), and nuclear PKA activity (C) upon stimulation of HEK293 cells with Iso (green circles), VIP (blue triangles), or NECA (pink squares) at the concentrations indicated. (D) Integrated signaling, calculated as the area under the curve after agonist addition, across doses of Iso, NECA, and VIP for all three biosensors. Corresponding time courses for a subset of data are shown in (A). Three-parameter dose-response curve fits are shown, and EC_{50}s are listed in Supplementary Table 1. For all panels, N = 2 (VIP cAMP at 1 μM and 10 pM) or N = 3 (all others) independent experiments, and error bars = S.D.

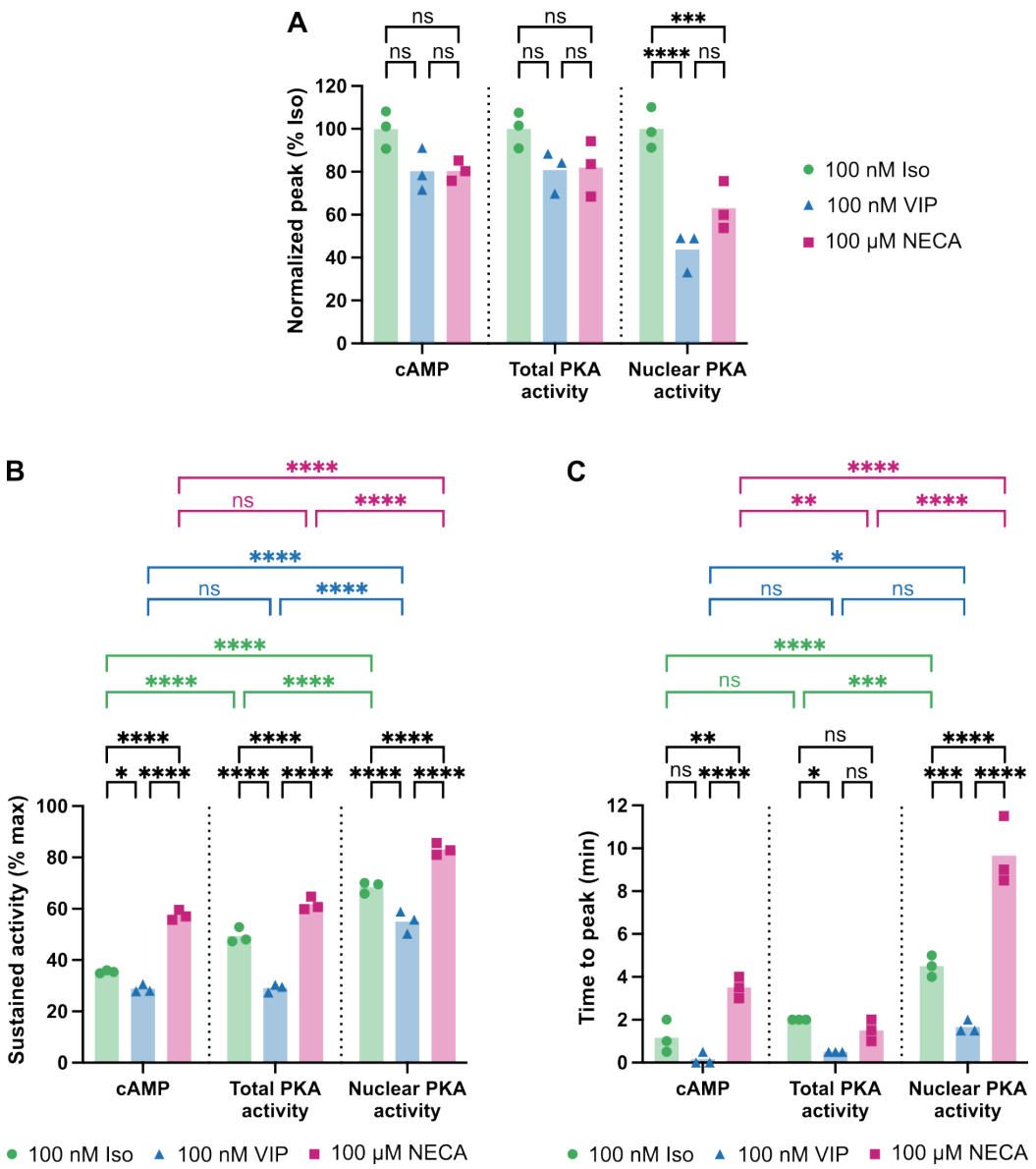

Supplementary Figure 5. Quantification of cAMP, total PKA activity, and nuclear PKA activity responses to saturating doses of agonist. (A) Peak responses upon stimulation with 100 nM Iso (green circles), 100 nM VIP (blue triangles) or 100 μM NECA (pink squares), normalized to the average peak response upon Iso stimulation. (B) Sustained activity, calculated as the percent peak signal remaining 30 minutes after agonist addition, across agonists and biosensors. (C) Time to peak responses upon agonist stimulation across the three biosensors. For all panels, biosensor fluorescence time courses are in Figure 2, N = 3 independent experiments, and significance was determined using ordinary 2-way ANOVA with Tukey's multiple comparisons test.

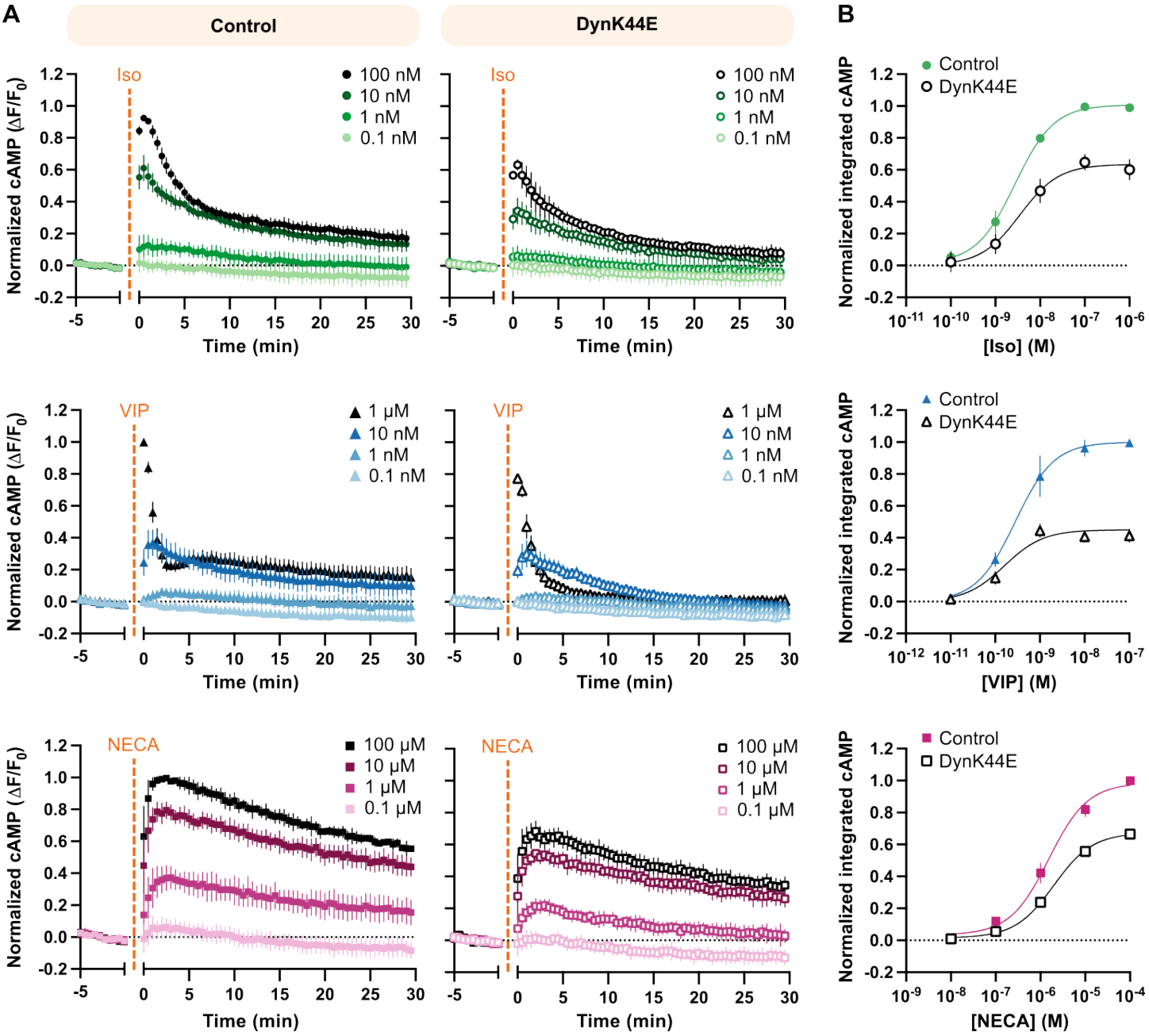

Supplementary Figure 6. cAMP biosensor dose-response curves with and without endocytic inhibition. (A) Fluorescence time courses of a cAMP biosensor in cells expressing mCherry (control, closed shapes) or mCherry-DynK44E (DynK44E, open shapes). Cells were treated with Iso (green circles), VIP (blue triangles), or NECA (pink squares) at the indicated concentrations. Within each agonist and biological replicate, data were normalized to the max response in control cells. (B) Integrated cAMP signaling, calculated as the area under the curve after agonist addition, for cells expressing control or DynK44E. Within each agonist and biological replicate, data were normalized to the largest response in control cells. Corresponding time courses for a subset of data are shown in (A). Three-parameter dose-response curve fits are shown, and EC_{50}s are listed in Supplementary Table 1. For all panels, N = 3 independent experiments, and error bars = S.D.

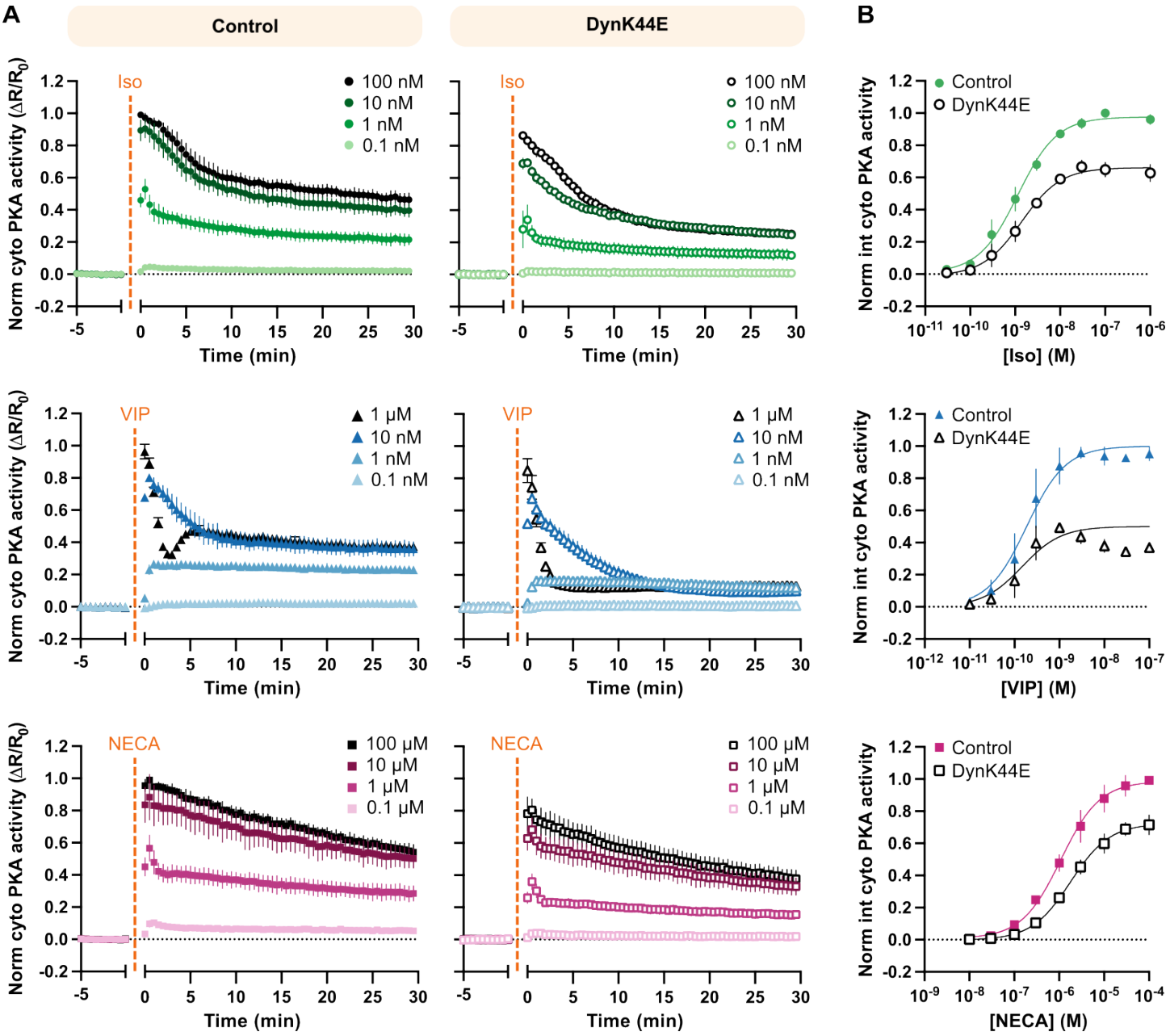

Supplementary Figure 7. Cytoplasmic PKA activity biosensor dose-response curves with and without endocytic inhibition. (A) Fluorescence time courses of a cytoplasmic PKA activity biosensor in cells expressing mCherry (control, closed shapes) or mCherry-DynK44E (DynK44E, open shapes). Cells were treated with Iso (green circles), VIP (blue triangles), or NECA (pink squares) at the indicated concentrations. Within each agonist and biological replicate, data were normalized to the max response in control cells. (B) Integrated cytoplasmic PKA activity, calculated as the area under the curve after agonist addition, for cells expressing control or DynK44E. Within each agonist and biological replicate, data were normalized to the largest response in control cells. Corresponding time courses for a subset of data are shown in (A). Three-parameter dose-response curve fits are shown, and EC_{50}s are listed in Supplementary Table 1. For all panels, N = 3 independent experiments, and error bars = S.D.

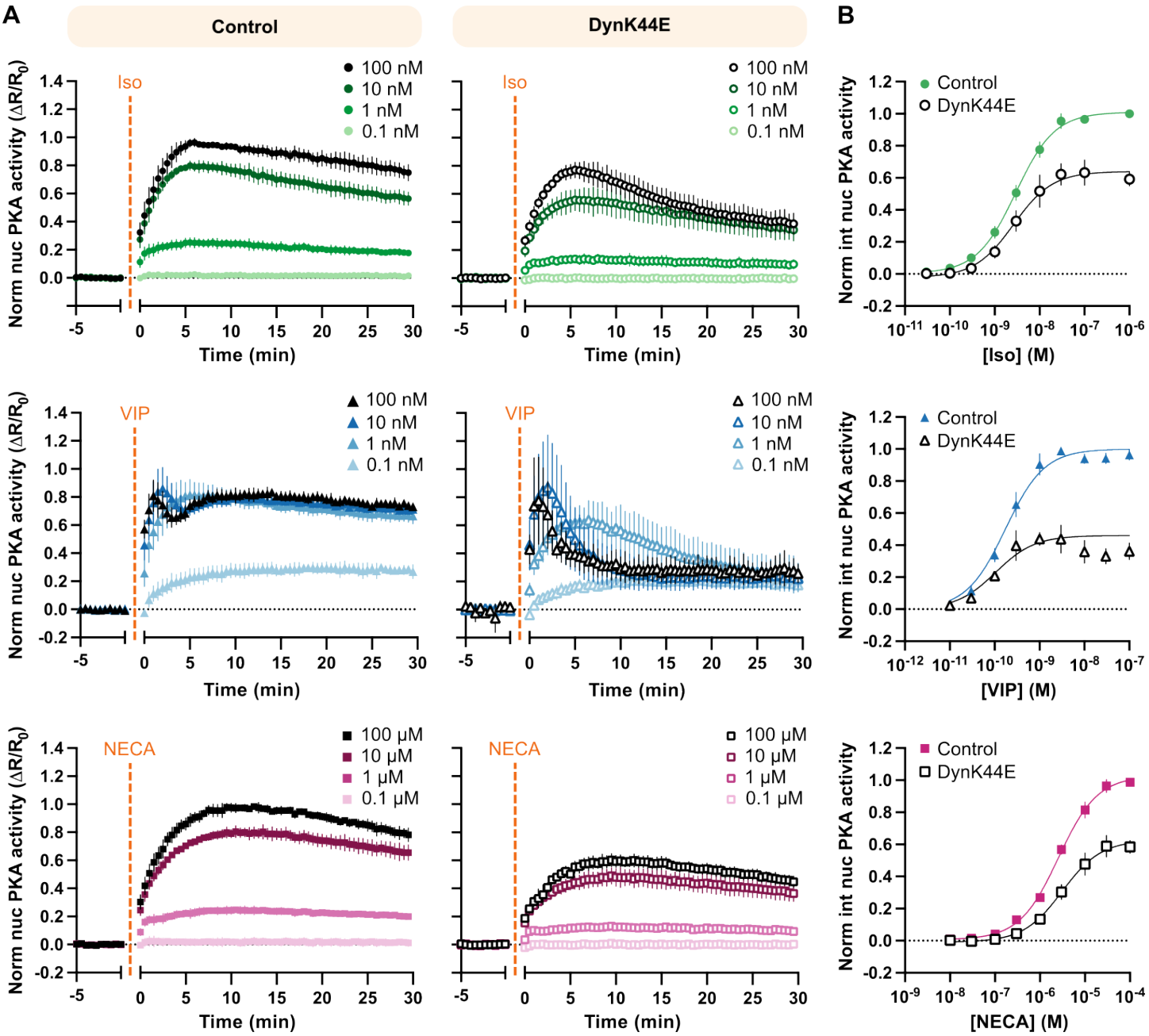

Supplementary Figure 8. Nuclear PKA activity biosensor dose-response curves with and without endocytic inhibition. (A) Fluorescence time courses of a nuclear PKA activity biosensor in cells expressing mCherry (control, closed shapes) or mCherry-DynK44E (DynK44E, open shapes). Cells were treated with Iso (green circles), VIP (blue triangles), or NECA (pink squares) at the indicated concentrations. Within each agonist and biological replicate, data were normalized to the max response in control cells. (B) Integrated nuclear PKA activity, calculated as the area under the curve after agonist addition, for cells expressing control or DynK44E. Within each agonist and biological replicate, data were normalized to the largest response in control cells. Corresponding time courses for a subset of data are shown in (A). Three-parameter dose-response curve fits are shown, and EC_{50}s are listed in Supplementary Table 1. For all panels, N = 3 independent experiments, and error bars = S.D.

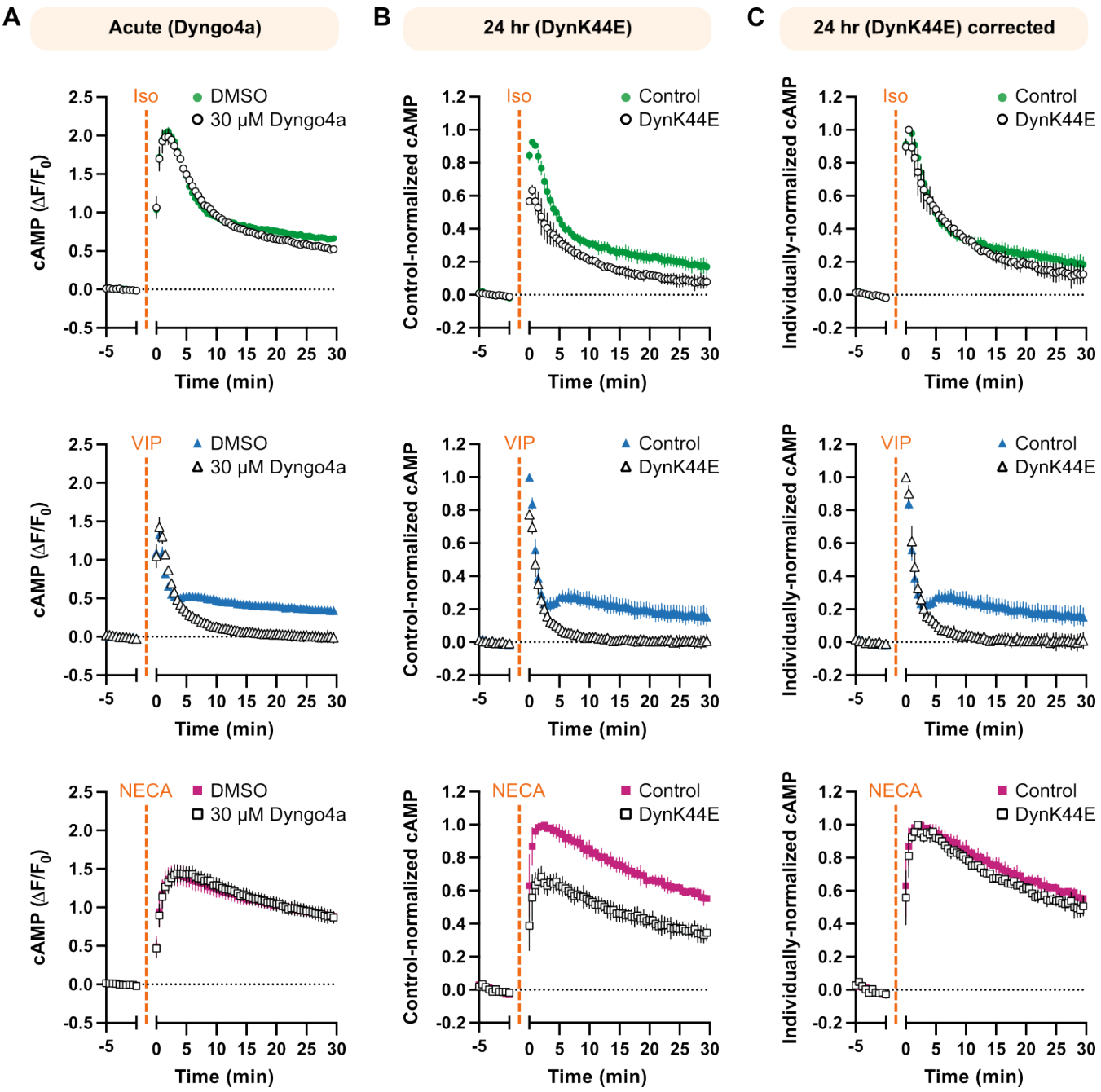

Supplementary Figure 9. Data normalization corrects for pleiotropic effects of prolonged endocytic inhibition. (A) Fluorescence time course of a cAMP biosensor in cells under acute endocytic inhibition. Cells were pretreated for 10 minutes with 30 μM Dyngo4a (open shapes) or DMSO (colored shapes) before stimulation with 100 nM Iso (green, circles), 100 nM VIP (blue, triangles), or 100 μM NECA (pink, squares). (B) Fluorescence time course of a cAMP biosensor in cells under 24 hours of endocytic inhibition. Cells expressing mCherry (control, closed shapes) or mCherry-DynK44E (DynK44E, open shapes) were stimulated with 100 nM Iso (green, circles), 100 nM VIP (blue, triangles), or 100 μM NECA (pink, squares). Within each agonist and biological replicate, data were normalized to the maximum response in control cells. Data are repeated from Supplementary Figure 6A. (C) Individually-normalized time courses from (B). Within each agonist, treatment, and biological replicate, data were normalized to the maximum response. Data are repeated from Figure 3A.

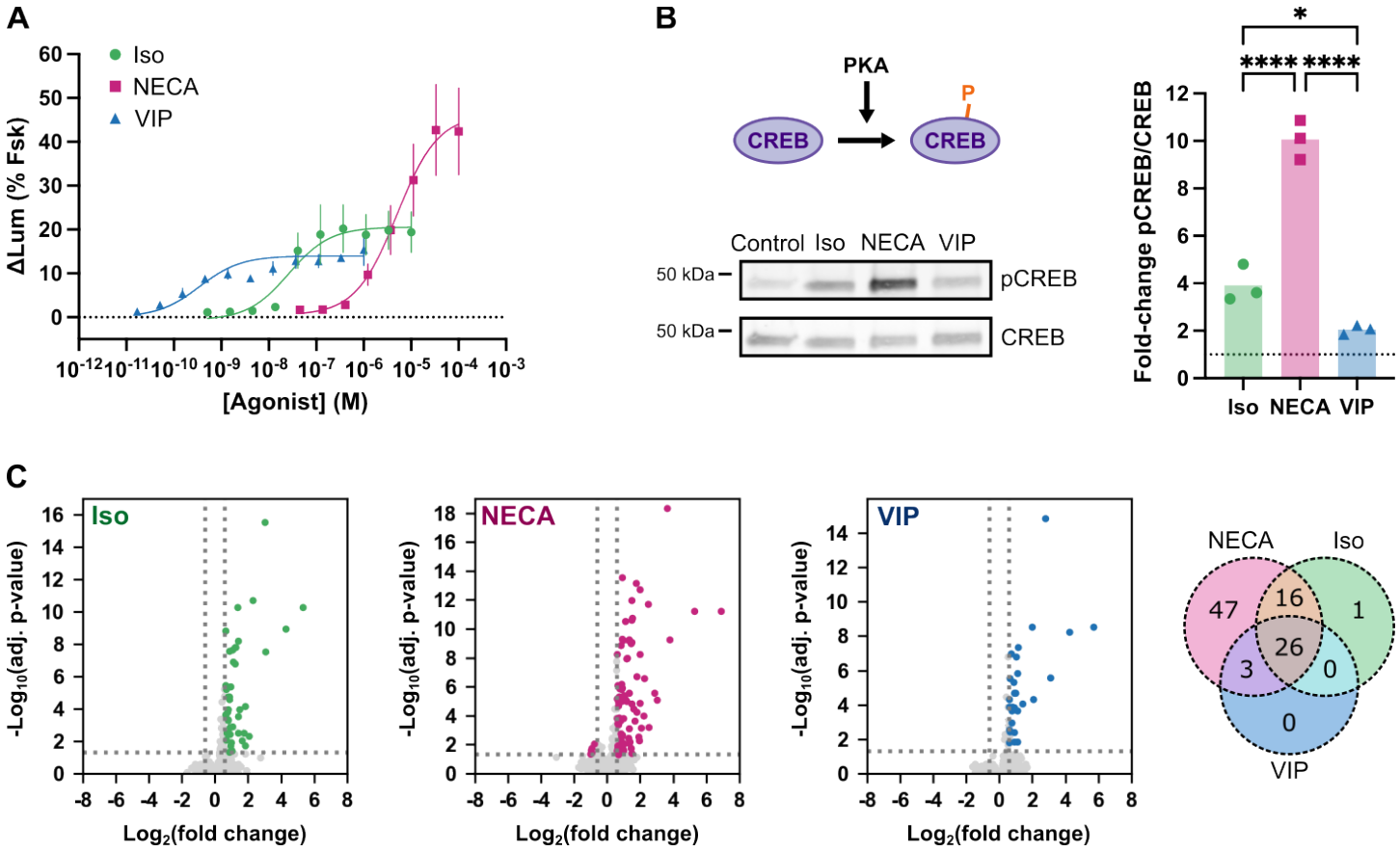

Supplementary Figure 10. Endogenous GPCRs elicit distinct transcriptional signatures. (A) Expression of CRE-luciferase transcriptional reporter upon treatment of cells with Iso (green circles), NECA (pink squares), or VIP (blue triangles) for 5 hours. Change in luminescence (ΔLum) was normalized to that of a forskolin-treated control within each replicate. Data with the highest agonist concentrations are repeated in Figure 6A. Three-parameter dose-response curve fits are shown, and EC_{50}s are listed in Supplementary Table 1. For all panels, N = 4 independent experiments, and error bars = S.D. (B) Representative western blot and quantification of phospho-CREB after 15 minute stimulation with 100 nM Iso (green circles), 100 μM NECA (pink squares), or 100 nM VIP (blue triangles). For quantification, the fold-change of pCREB was normalized to total CREB. Results from three independent experiments are shown. Significance was determined by ordinary one-way ANOVA with Tukey's multiple comparisons test. (C) Differential gene expression analysis from RNA-seq data. Cells were treated with agonist or corresponding vehicle (100 nM Iso, 20 μM NECA, or 500 nM VIP) for 90 minutes. Significantly changing genes, indicated by colored points, have adjusted p-value < 0.05 and fold-change > 1.5 (dotted lines). Venn diagram summarizes gene overlap, and a full list of significant genes can be found in Supplementary Table 3.

Supplementary Tables

Supplementary Table 1. Agonist EC_{50}s.

Agonist	Biosensor	Pre-treatment	pEC_{50}	95% CI
Iso	cAMP	None	8.6	8.5 - 8.8
	Total PKA		8.4	8.3 - 8.5
	Nuclear PKA		8.4	8.3 - 8.5
	CRE-luciferase		7.6	7.3 - 7.8
	cAMP	mCherry	8.6	8.5 - 8.7
	Cytoplasmic PKA		8.9	8.8 - 9.0
	Nuclear PKA		8.5	8.5 - 8.6
	CRE-luciferase		7.3	7.1 - 7.5
	cAMP	mCherry-DynK44E	8.5	8.2 - 8.7
	Cytoplasmic PKA		8.9	8.7 - 9.0
	Nuclear PKA		8.6	8.4 - 8.7
	CRE-luciferase		7.2	6.9 - 7.5
VIP	cAMP	None	9.8	9.6 - 10.0
	Total PKA		8.5	8.2 - 8.7
	Nuclear PKA		7.8	7.6 - 8.0
	CRE-luciferase		9.6	9.2 - 9.7
	cAMP	mCherry	9.6	9.4 - 9.7
	Cytoplasmic PKA		9.7	9.6 - 9.8
	Nuclear PKA		9.8	9.7 - 9.8
	CRE-luciferase		9.6	9.5 - 9.8
	cAMP	mCherry-DynK44E	9.8	9.6 - 10.0
	Cytoplasmic PKA		9.8	9.6 - 10.1
	Nuclear PKA		10	9.7 - 10.2
	CRE-luciferase		10.1	9.8 - 10.5
NECA	cAMP	None	5.8	5.7 - 5.9
	Total PKA		5.6	5.5 - 5.7
	Nuclear PKA		5.5	5.4 - 5.7
	CRE-luciferase		5.3	5.1 - 5.5
	cAMP	mCherry	5.8	5.7 - 6.0
	Cytoplasmic PKA		6.0	5.9 - 6.1
	Nuclear PKA		5.6	5.5 - 5.6
	CRE-luciferase		5.4	5.2 - 5.5
	cAMP	mCherry-DynK44E	5.7	5.6 - 5.8
	Cytoplasmic PKA		5.7	5.7 - 5.8
	Nuclear PKA		5.5	5.4 - 5.6
	CRE-luciferase		5.3	5.1 - 5.5

Supplementary Table 2. Estimated signaling decay constants. NA = could not be fit to single exponential decay.

Agonist	Biosensor	k (s^{-1})	95% CI (s^{-1})	Timepoints fit
Iso	cAMP	0.14	0.12 - 0.16	2.5 - 29.5 min
	PKA activity	0.12	0.093 - 0.15	3 - 29.5 min
	Nuclear PKA activity	0.064	0.014 - 0.12	5 - 29.5 min
NECA	cAMP	0.019	0.0048 - 0.033	4 - 29.5 min
	PKA activity	NA	NA	NA
	Nuclear PKA activity	NA	NA	NA
VIP	cAMP	0.53	0.13 - 1.0	0.5 - 4 min
	PKA activity	0.44	0.13 - 0.81	0.5 -5 min
	Nuclear PKA activity	0.4	0.16 - 0.76	2 - 14.5 min

Supplementary Table 3. Genes differentially expressed upon Iso, VIP, or NECA treatment.

Differentially expressed genes upon treatment with 100 nM Iso

Gene ID	Gene Name	Description	Log2FC	adj p-value	Shared with VIP?	Shared with NECA?	Previously identified Iso target (ref 49)?	Annotated CREB target (ref 50)?
ENSG00000124253	PCK1	phosphoenolpyruvate carboxykinase 1	5.31	5.06E-11	Y	Y	Y	Y
ENSG00000119508	NR4A3	nuclear receptor subfamily 4 group A member 3	4.28	1.09E-09	Y	Y	N	Y
ENSG00000123358	NR4A1	nuclear receptor subfamily 4 group A member 1	3.08	2.79E-08	Y	Y	Y	Y
ENSG00000153234	NR4A2	nuclear receptor subfamily 4 group A member 2	3.02	2.86E-16	Y	Y	Y	Y
ENSG00000135346	CGA	glycoprotein hormones, alpha polypeptide	2.29	2.01E-11	Y	Y	Y	Y
ENSG00000122641	INHBA	inhibin subunit beta A	2.05	4.81E-03	N	Y	N	Y
ENSG00000109321	AREG	amphiregulin	1.82	6.92E-05	Y	Y	N	Y
ENSG00000125740	FOSB	FosB proto-oncogene, AP-1 transcription factor subunit	1.82	1.85E-02	N	Y	N	Y
ENSG00000186352	ANKRD37	ankyrin repeat domain 37	1.75	3.10E-03	N	Y	Y	N
ENSG00000171951	SCG2	secretogranin II	1.64	8.89E-03	N	Y	N	Y
ENSG00000073756	PTGS2	prostaglandin-endoperoxide synthase 2	1.48	1.13E-04	Y	Y	N	Y
ENSG00000176907	TCIM	transcriptional and immune response regulator	1.41	3.03E-04	Y	Y	N	N
ENSG00000159388	BTG2	BTG anti-proliferation factor 2	1.41	6.05E-09	Y	Y	N	Y
ENSG00000133636	NTS	neurotensin	1.40	3.10E-03	N	Y	Y	Y
ENSG00000187479	C11orf96	chromosome 11 open reading frame 96	1.38	5.06E-11	Y	Y	N	N
ENSG00000120129	DUSP1	dual specificity phosphatase 1	1.24	1.55E-08	Y	Y	Y	Y
ENSG00000196352	CD55	CD55 molecule (Cromer blood group)	1.22	1.58E-07	Y	Y	Y	N
ENSG00000059804	SLC2A3	solute carrier family 2 member 3	1.20	1.55E-08	Y	Y	Y	Y
ENSG00000143878	RHOB	ras homolog family member B	1.09	1.21E-07	Y	Y	N	N
ENSG00000130844	ZNF331	zinc finger protein 331	1.06	2.24E-08	Y	Y	N	Y
ENSG00000171223	JUNB	JunB proto-oncogene, AP-1 transcription factor subunit	1.05	1.29E-03	Y	Y	Y	Y
ENSG00000139318	DUSP6	dual specificity phosphatase 6	1.02	4.05E-02	N	Y	N	Y
ENSG00000125968	ID1	inhibitor of DNA binding 1, HLH protein	0.99	1.18E-02	N	N	N	Y
ENSG00000120875	DUSP4	dual specificity phosphatase 4	0.95	1.94E-02	N	Y	N	Y
ENSG00000157514	TSC22D3	TSC22 domain family member 3	0.94	4.24E-06	Y	Y	N	N
ENSG00000155592	ZKSCAN2	zinc finger with KRAB and SCAN domains 2	0.90	3.86E-03	Y	Y	N	N
ENSG00000198517	MAFK	MAF bZIP transcription factor K	0.89	1.44E-03	N	Y	N	Y
ENSG00000162772	ATF3	activating transcription factor 3	0.88	2.64E-08	Y	Y	Y	Y
ENSG00000137449	CPEB2	cytoplasmic polyadenylation element binding protein 2	0.86	4.63E-02	N	Y	N	Y
ENSG00000164778	EN2	engrailed homeobox 2	0.86	1.75E-05	Y	Y	Y	Y
ENSG00000118985	ELL2	elongation factor for RNA polymerase II 2	0.86	2.51E-05	Y	Y	Y	Y
ENSG00000116741	RGS2	regulator of G protein signaling 2	0.85	3.89E-03	N	Y	N	Y
ENSG00000198435	NRARP	NOTCH regulated ankyrin repeat protein	0.80	1.83E-05	N	Y	N	N
ENSG00000075426	FOSL2	FOS like 2, AP-1 transcription factor subunit	0.80	5.26E-04	Y	Y	Y	Y

ENSG00000185112	FAM43A	family with sequence similarity 43 member A	0.79	1.14E-04	N	Y	Y	N
ENSG00000180730	SHISA2	shisa family member 2	0.78	4.83E-04	Y	Y	N	N
ENSG00000087510	TFAP2C	transcription factor AP-2 gamma	0.75	1.54E-04	Y	Y	N	Y
ENSG00000170525	PFKFB3	6-phosphofructo-2-kinase/fructose-2,6-biphosphatase 3	0.70	2.99E-03	N	Y	N	Y
ENSG00000186480	INSIG1	insulin induced gene 1	0.67	5.95E-06	Y	Y	N	Y
ENSG00000095794	CREM	cAMP responsive element modulator	0.66	8.49E-03	N	Y	Y	Y
ENSG00000185650	ZFP36L1	ZFP36 ring finger protein like 1	0.64	2.28E-04	N	Y	N	Y
ENSG00000169895	SYAP1	synapse associated protein 1	0.62	1.45E-09	N	Y	Y	Y
ENSG00000112773	TENT5A	terminal nucleotidyltransferase 5A	0.62	3.42E-06	Y	Y	N	N

Differentially expressed genes upon treatment with 500 nM VIP

Gene ID	Gene Name	Description	Log2FC	adj p-value	Shared with Iso?	Shared with NECA?	Previously identified Iso target (ref 49)?	Annotated CREB target (ref 50)?
ENSG00000124253	PCK1	phosphoenolpyruvate carboxykinase 1	5.70	2.86E-09	Y	Y	Y	Y
ENSG00000119508	NR4A3	nuclear receptor subfamily 4 group A member 3	4.26	5.74E-09	Y	Y	N	Y
ENSG00000123358	NR4A1	nuclear receptor subfamily 4 group A member 1	3.09	2.58E-06	Y	Y	Y	Y
ENSG00000153234	NR4A2	nuclear receptor subfamily 4 group A member 2	2.79	1.36E-15	Y	Y	Y	Y
ENSG00000109321	AREG	amphiregulin	2.06	4.63E-05	Y	Y	N	Y
ENSG00000135346	CGA	glycoprotein hormones, alpha polypeptide	1.99	2.86E-09	Y	Y	Y	Y
ENSG00000073756	PTGS2	prostaglandin-endoperoxide synthase 2	1.42	8.91E-05	Y	Y	N	Y
ENSG00000120129	DUSP1	dual specificity phosphatase 1	1.15	4.43E-08	Y	Y	Y	Y
ENSG00000159388	BTG2	BTG anti-proliferation factor 2	1.11	1.42E-06	Y	Y	N	Y
ENSG00000155592	ZKSCAN2	zinc finger with KRAB and SCAN domains 2	1.11	2.23E-04	Y	Y	N	N
ENSG00000176907	TCIM	transcriptional and immune response regulato	1.10	1.48E-02	Y	Y	N	N
ENSG00000187479	C11orf96	chromosome 11 open reading frame 96	1.01	1.64E-07	Y	Y	N	N
ENSG00000196352	CD55	CD55 molecule (Cromer blood group)	0.99	2.11E-05	Y	Y	Y	N
ENSG00000171223	JUNB	JunB proto-oncogene, AP-1 transcription factor subunit	0.91	1.48E-02	Y	Y	Y	Y
ENSG00000112541	PDE10A	phosphodiesterase 10A	0.91	4.15E-03	N	Y	N	Y
ENSG00000075426	FOSL2	FOS like 2, AP-1 transcription factor subunit	0.90	1.51E-04	Y	Y	Y	Y
ENSG00000143878	RHOB	ras homolog family member B	0.89	2.11E-05	Y	Y	N	N
ENSG00000130844	ZNF331	zinc finger protein 331	0.86	4.83E-06	Y	Y	N	Y
ENSG00000157514	TSC22D3	TSC22 domain family member 3	0.80	1.37E-04	Y	Y	N	N
ENSG00000059804	SLC2A3	solute carrier family 2 member 3	0.77	2.31E-04	Y	Y	Y	Y
ENSG00000180730	SHISA2	shisa family member 2	0.76	1.14E-03	Y	Y	N	N
ENSG00000087510	TFAP2C	transcription factor AP-2 gamma	0.74	1.51E-04	Y	Y	N	Y
ENSG00000154734	ADAMTS1	ADAM metallopeptidase with thrombospondin type 1 motif 1	0.71	1.04E-07	N	Y	Y	Y
ENSG00000164778	EN2	engrailed homeobox 2	0.64	3.58E-03	Y	Y	Y	Y
ENSG00000112773	TENT5A	terminal nucleotidyltransferase 5A	0.63	2.94E-06	Y	Y	N	N

ENSG00000141232	TOB1	transducer of ERBB2, 1	0.61	2.84E-03	N	Y	N	Y
ENSG00000186480	INSIG1	insulin induced gene 1	0.61	4.87E-05	Y	Y	N	Y
ENSG00000162772	ATF3	activating transcription factor 3	0.59	1.31E-04	Y	Y	Y	Y
ENSG00000118985	ELL2	elongation factor for RNA polymerase II 2	0.59	1.55E-02	Y	Y	Y	Y

Differentially expressed genes upon treatment with 20 µM NECA

Gene ID	Gene Name	Description	Log2FC	adj p-value	Shared with Iso?	Shared with VIP?	Previously identified Iso target (ref 49)?	Annotated CREB target (ref 50)?
ENSG00000124253	PCK1	phosphoenolpyruvate carboxykinase 1	6.88	5.96E-12	Y	Y	Y	Y
ENSG00000119508	NR4A3	nuclear receptor subfamily 4 group A member 3	5.30	5.96E-12	Y	Y	N	Y
ENSG00000123358	NR4A1	nuclear receptor subfamily 4 group A member 1	3.80	5.62E-10	Y	Y	Y	Y
ENSG00000153234	NR4A2	nuclear receptor subfamily 4 group A member 2	3.64	4.45E-19	Y	Y	Y	Y
ENSG00000125740	FOSB	FosB proto-oncogene, AP-1 transcription factor subunit	3.02	8.28E-06	Y	N	N	Y
ENSG00000186352	ANKRD37	ankyrin repeat domain 37	2.88	2.73E-06	Y	N	Y	N
ENSG00000179388	EGR3	early growth response 3	2.53	6.25E-04	N	N	N	Y
ENSG00000135346	CGA	glycoprotein hormones, alpha polypeptide	2.50	1.96E-12	Y	Y	Y	Y
ENSG00000109321	AREG	amphiregulin	2.24	2.75E-07	Y	Y	N	Y
ENSG00000171951	SCG2	secretogranin II	2.21	1.04E-04	Y	N	N	Y
ENSG00000119986	AVPI1	arginine vasopressin induced 1	2.07	6.89E-04	N	N	Y	N
ENSG00000159388	BTG2	BTG anti-proliferation factor 2	2.00	1.94E-13	Y	N	N	Y
ENSG00000171223	JUNB	JunB proto-oncogene, AP-1 transcription factor subunit	1.98	5.69E-09	Y	Y	Y	Y
ENSG00000133636	NTS	neurotensin	1.98	1.30E-05	Y	N	Y	Y
ENSG00000211448	DIO2	iodothyronine deiodinase 2	1.93	5.15E-03	N	N	N	Y
ENSG00000122641	INHBA	inhibin subunit beta A	1.91	3.01E-03	Y	N	N	Y
ENSG00000073756	PTGS2	prostaglandin-endoperoxide synthase 2	1.78	2.05E-07	Y	Y	N	Y
ENSG00000275202		novel transcript, antisense to FNDC3A	1.77	5.51E-05	N	N	N	NA
ENSG00000187479	C11orf96	chromosome 11 open reading frame 96	1.76	6.86E-14	Y	Y	N	N
ENSG00000164283	ESM1	endothelial cell specific molecule 1	1.67	2.37E-04	N	N	N	Y
ENSG00000176907	TCIM	transcriptional and immune response regulator	1.58	3.44E-05	Y	N	N	N
ENSG00000059804	SLC2A3	solute carrier family 2 member 3	1.52	1.75E-11	Y	Y	Y	Y
ENSG00000148057	IDNK	IDNK gluconokinase	1.50	4.15E-02	N	N	N	N
ENSG00000120129	DUSP1	dual specificity phosphatase 1	1.49	2.39E-11	Y	Y	Y	Y
ENSG00000130844	ZNF331	zinc finger protein 331	1.49	1.06E-12	Y	Y	N	Y
ENSG00000075426	FOSL2	FOS like 2, AP-1 transcription factor subunit	1.48	8.15E-10	Y	Y	Y	Y
ENSG00000120875	DUSP4	dual specificity phosphatase 4	1.48	1.51E-05	Y	N	N	Y
ENSG00000133874	RNF122	ring finger protein 122	1.46	1.71E-02	N	N	Y	Y
ENSG00000196352	CD55	CD55 molecule (Cromer blood group)	1.46	1.03E-09	Y	Y	Y	N
ENSG00000095752	IL11	interleukin 11	1.36	6.58E-03	N	N	N	Y

ENSG00000155592	ZKSCAN2	zinc finger with KRAB and SCAN domains 2	1.34	2.74E-06	Y	Y	N	N
ENSG00000182372	CLN8	CLN8 transmembrane ER and ERGIC protein	1.33	7.87E-04	N	N	N	Y
ENSG00000143878	RHOB	ras homolog family member B	1.33	5.62E-10	Y	Y	N	N
ENSG00000128594	LRRC4	leucine rich repeat containing 4	1.31	7.69E-03	N	N	N	N
ENSG00000118985	ELL2	elongation factor for RNA polymerase II 2	1.29	6.05E-10	Y	Y	Y	Y
ENSG00000139318	DUSP6	dual specificity phosphatase 6	1.27	3.67E-03	Y	N	N	Y
ENSG00000157514	TSC22D3	TSC22 domain family member 3	1.22	1.04E-08	Y	Y	N	N
ENSG00000164778	EN2	engrailed homeobox 2	1.17	1.17E-08	Y	Y	Y	Y
ENSG00000198517	MAFK	MAF bZIP transcription factor K	1.16	9.76E-06	Y	N	N	Y
ENSG00000162772	ATF3	activating transcription factor 3	1.11	2.98E-11	Y	Y	Y	Y
ENSG00000147894	C9orf72	C9orf72-SMCR8 complex subunit	1.11	7.32E-06	N	N	N	N
ENSG00000180730	SHISA2	shisa family member 2	1.02	4.24E-06	Y	Y	N	N
ENSG00000095794	CREM	cAMP responsive element modulator	1.02	6.01E-06	Y	N	Y	Y
ENSG00000272512		novel transcript	1.01	8.84E-03	N	N	N	NA
ENSG00000176697	BDNF	brain derived neurotrophic factor	0.99	2.46E-02	N	N	N	Y
ENSG00000116741	RGS2	regulator of G protein signaling 2	0.99	1.50E-04	Y	N	N	Y
ENSG00000125812	GZF1	GDNF inducible zinc finger protein 1	0.99	2.46E-02	N	N	N	N
ENSG00000137449	CPEB2	cytoplasmic polyadenylation element binding protein 2	0.97	8.45E-03	Y	N	N	Y
ENSG00000186480	INSIG1	insulin induced gene 1	0.96	6.05E-10	Y	Y	N	Y
ENSG00000142871	CCN1	cellular communication network factor 1	0.92	1.18E-06	N	N	N	N
ENSG00000112773	TENT5A	terminal nucleotidyltransferase 5A	0.91	4.84E-10	Y	Y	N	N
ENSG00000112541	PDE10A	phosphodiesterase 10A	0.91	2.18E-03	N	Y	N	Y
ENSG00000169895	SYAP1	synapse associated protein 1	0.91	2.68E-14	Y	N	Y	Y
ENSG00000118515	SGK1	serum/glucocorticoid regulated kinase 1	0.90	1.06E-02	N	N	N	N
ENSG00000198455	ZXDB	zinc finger X-linked duplicated B	0.89	2.43E-02	N	N	N	N
ENSG00000198435	NRARP	NOTCH regulated ankyrin repeat protein	0.88	1.43E-06	Y	N	N	N
ENSG00000132906	CASP9	caspase 9	0.87	1.20E-02	N	N	Y	Y
ENSG00000185112	FAM43A	family with sequence similarity 43 member A	0.86	9.90E-06	Y	N	Y	N
ENSG00000013588	GPRC5A	G protein-coupled receptor class C group 5 member A	0.86	6.62E-07	N	N	N	N
ENSG00000169067	ACTBL2	actin beta like 2	0.86	1.49E-02	N	N	N	N
ENSG00000144655	CSRNP1	cysteine and serine rich nuclear protein 1	0.86	2.93E-03	N	N	N	N
ENSG00000092421	SEMA6A	semaphorin 6A	0.86	6.72E-03	N	N	N	Y
ENSG00000185650	ZFP36L1	ZFP36 ring finger protein like 1	0.86	1.23E-06	Y	N	N	Y
ENSG00000087510	TFAP2C	transcription factor AP-2 gamma	0.85	4.74E-06	Y	Y	N	Y
ENSG00000113448	PDE4D	phosphodiesterase 4D	0.82	1.75E-03	N	N	N	Y
ENSG00000154734	ADAMTS1	ADAM metallopeptidase with thrombospondin type 1 motif 1	0.81	1.45E-09	N	Y	Y	Y
ENSG00000104419	NDRG1	N-myc downstream regulated 1	0.80	1.65E-04	N	N	N	Y
ENSG00000170525	PFKFB3	6-phosphofructo-2-kinase/fructose-2,6-biphosphatase 3	0.78	2.40E-04	Y	N	N	Y
ENSG00000139112	GABARAPL1	GABA type A receptor associated protein like 1	0.76	1.34E-06	N	N	N	Y

ENSG00000255112	CHMP1B	charged multivesicular body protein 1B	0.75	5.12E-06	N	N	Y	N
ENSG00000141232	TOB1	transducer of ERBB2, 1	0.73	1.43E-04	N	Y	N	Y
ENSG00000124225	PMEPA1	prostate transmembrane protein, androgen induced	0.71	5.02E-06	N	N	Y	N
ENSG00000141582	CBX4	chromobox 4	0.69	1.16E-05	N	N	N	Y
ENSG00000125845	BMP2	bone morphogenetic protein 2	0.68	4.57E-02	N	N	Y	Y
ENSG00000113070	HBEGF	heparin binding EGF like growth factor	0.68	3.33E-02	N	N	N	N
ENSG00000186977	KRTAP19-5	keratin associated protein 19-5	0.67	4.69E-02	N	N	N	Y
ENSG00000204186	ZDBF2	zinc finger DBF-type containing 2	0.66	4.27E-04	N	N	N	N
ENSG00000188042	ARL4C	ADP ribosylation factor like GTPase 4C	0.66	1.95E-05	N	N	N	N
ENSG00000119866	BCL11A	BAF chromatin remodeling complex subunit BCL11A	0.66	3.39E-04	N	N	N	Y
ENSG00000112715	VEGFA	vascular endothelial growth factor A	0.64	2.62E-02	N	N	N	N
ENSG00000120149	MSX2	msh homeobox 2	0.63	1.15E-02	N	N	N	Y
ENSG00000115738	ID2	inhibitor of DNA binding 2	0.62	8.40E-07	N	N	N	Y
ENSG00000162924	REL	REL proto-oncogene, NF-kB subunit	0.62	1.71E-02	N	N	N	Y
ENSG00000133639	BTG1	BTG anti-proliferation factor 1	0.61	5.64E-09	N	N	N	Y
ENSG00000165030	NFIL3	nuclear factor, interleukin 3 regulated	0.61	2.62E-02	N	N	Y	Y
ENSG00000177508	IRX3	iroquois homeobox 3	0.61	1.50E-04	N	N	N	N
ENSG00000069849	ATP1B3	ATPase Na+/K+ transporting subunit beta 3	0.60	6.69E-06	N	N	Y	Y
ENSG00000265972	TXNIP	thioredoxin interacting protein	-0.78	8.62E-03	N	N	N	Y
ENSG00000103460	TOX3	TOX high mobility group box family member 3	-0.93	1.73E-02	N	N	N	N
ENSG00000147118	ZNF182	zinc finger protein 182	-0.95	3.80E-02	N	N	N	N
ENSG00000232040	ZBED9	zinc finger BED-type containing 9	-0.98	2.52E-02	N	N	N	N
ENSG00000109674	NEIL3	nei like DNA glycosylase 3	-1.02	4.35E-02	N	N	N	N

Supplementary Table 4. Chemicals used in this study.

Chemical	Manufacturer	Catalog #	Solvent
(-)-Isoproterenol hydrochloride	Millipore Sigma	I6504	100 mM L-ascorbic acid
NECA (5'-N-Ethylcarboxamidoadenosine)	Tocris Bioscience	1691	DMSO
CGS-21680 hydrochloride	Tocris Bioscience	1063	DMSO
VIP (vasoactive intestinal peptide)	Tocris Bioscience	1911	Water
Forskolin	Millipore Sigma	F6886	DMSO
Alexa Fluor 647 Protein Labeling Kit	Invitrogen	A20173	NA
JF635i-HTL	gift from Luke Lavis	NA	DMSO
D-luciferin	Gold Biotechnology	LUCNA	10 mM HEPES pH 7.4
Alprenolol hydrochloride	Millipore Sigma	A0360000	100 mM L-ascorbic acid
CGP 20712 dihydrochloride	Tocris Bioscience	1024	Water
ICI 118551 hydrochloride	Cayman Chemical	15591	DMSO

Supplementary Table 5. Antibodies used in this study

Antibody	Manufacturer	Catalog #	Use	Dilution
mouse anti-CREB (86B10)	Cell Signaling Technologies	9104	Western Blot	1:1000
rabbit anti-phosphoCREB (S133) (87G3)	Cell Signaling Technologies	9198	Western Blot	1:1000
IRDye 680RD donkey anti-rabbit IgG	LI-COR Biosciences	926-68073	Western Blot	1:10000
IRDye 800CW donkey anti-mouse IgG	LI-COR Biosciences	926-32212	Western Blot	1:10000
mouse anti-FLAG (M1)	Millipore Sigma	F3040	Live Cell Imaging, Flow Cytometry	1:1000

Supplementary Table 6. DNA constructs and BacMam viruses used in this study.

Construct	Source
pCMV-Dest_ExRai-AKAR2	This study; insertion of ExRai-AKAR2 into pCMV-Dest (Invitrogen A24223) between Gateway sites. ExRai-AKAR2 was a gift from Jin Zhang (Addgene plasmid #161753)
pCMV-Dest-ExRai-AKAR2-NES	This study; insertion of ExRai-AKAR2-NES (ref 39) into pCMV-Dest (Invitrogen A24223) between Gateway sites.
pCMV-Dest_ExRai-AKAR2-NLS	This study; insertion of ExRai-AKAR2-NLS (ref 39) into pCMV-Dest (Invitrogen A24223) between Gateway sites.
pCMV-Dest-mCherry	(ref 20)
pCMV-Dest-mCherry-DynK44E	(ref 20)
pGL4.29[*luc2P*/CRE/Hygro]	Promega E8471
pcDNA3.1-SS-FLAG-A2BR	This study; insertion of A2BR (cDNA Resource Center #ADRA2BTN00) into pcDNA3.1 at HindIII/XbaI with N-terminal sequence added: MKTIIALSYIFCLVFADYKDDDDAAAAGGGSGS
pcDNA3.1-SS-HaloTag-A2BR	This study; replacement of FLAG-linker (DYKDDDDAAAAGGGSGS) with HaloTag7 in pcDNA3.1-SS-FLAG-A2BR, flanked by GS (N-term) and GGGGSGS (C-term)
pcDNA3.1-SS-FLAG-VIPR1	(ref 20)
pcDNA-SS-FLAG-β2AR	(ref 51)
pVenus-NES-Venus-miniGs	(ref 28)
CMV-cADDis Green Up	Montana Molecular #U0200G